Production of bottomonia states in proton-proton and heavy ion collisions

Vineet Kumar[d,*], Prashant Shukla[d,f], Abhijit Bhattacharyya[e]

[a]*Nuclear Physics Division, Bhabha Atomic Research Centre, Mumbai 400085, India*
[b]*Department of Physics, University of Calcutta, 92, A. P. C. Road Kolkata-700009, India*
[c]*Homi Bhabha National Institute, Anushakti Nagar, Mumbai 400094, India*

Abstract

This work reviews the study of bottomonia production in high energy hadronic collisions to investigate the fundamental aspects of Quantum Chromodynamics. Emphasis is given to the lessons learnt from the LHC data, which are reviewed in a global prospective with the results from the RHIC at lower energies used for comparison. The review covers bottomonia production in proton-proton, proton-nucleus and nucleus-nucleus collisions and includes discussion of the effects of hot and cold strongly interacting matter.

Keywords: Beauty, Quarkonium, Hadron Collision, Heavy-Ion Collision, Quark-Gluon Plasma, LHC, RHIC

Contents

*Corresponding author
Email address: vineetk@barc.gov.in (Vineet Kumar)

Production of bottomonia states in proton-proton and heavy ion collisions

Vineet Kumar[d,*], Prashant Shukla[d,f], Abhijit Bhattacharyya[e]

[d]*Nuclear Physics Division, Bhabha Atomic Research Centre, Mumbai 400085, India*
[e]*Department of Physics, University of Calcutta, 92, A. P. C. Road Kolkata-700009, India*
[f]*Homi Bhabha National Institute, Anushakti Nagar, Mumbai 400094, India*

1. Introduction

It is expected that strongly-interacting matter shows qualitatively new behavior at temperatures and/or densities which are comparable to or larger than the typical hadronic scale. It has been argued that under such extreme conditions deconfinement of quarks and gluons should set in and the thermodynamics of strongly-interacting matter could then be understood in terms of these elementary degrees of freedom. This new form of matter is called quark-gluon plasma [1, 2], or QGP. The existence of such a transition has indeed been demonstrated from first principles using Monte Carlo simulations of lattice QCD. The deconfinement transition and the properties of hot, strongly-interacting matter can be studied experimentally in heavy-ion collisions [3]. A significant part of the extensive experimental heavy-ion program is dedicated to measuring quarkonium yields since Matsui and Satz suggested that quarkonium suppression could be a signature of deconfinement [4].

In fact, the observation of anomalous suppression was considered to be a key signature of deconfinement at SPS energies [5].

2. Bottomonia production mechanism in p-p collisions

In general one can subdivide the quarkonia production process into two major parts

1. Production of a heavy quark pair in hard collisions.
2. Formation of quarkonia out of the two heavy quarks.

First process can be calculated by the perturbative QCD calculations while the formation of quarkonia out of the two heavy quarks is a non perturbative process and require some effective theories for modelling.

*Corresponding author
Email address: vineetk@barc.gov.in (Vineet Kumar)

2.1. Production of a heavy quark pair in hard collisions

Due to the high mass of the heavy quarks ($m_c \sim 1.3$ GeV/c^2, $m_b \sim 4.7$ GeV/c^2), they can be produced only during the first phase of a collision. Only at that time the elementary collisions with sufficiently high momentum transfers (to create such high masses) takes place. For this reason the heavy quark production is a hard process that can be treated perturbatively. The hadronic cross section in pp collisions can be written as

$$\sigma_{pp}(s, m^2) = \sum_{i,j=q,\bar{q},g} \int dx_1\, dx_2\, f_i^p(x_1, \mu_F^2)\, f_j^p(x_2, \mu_F^2)\, \widehat{\sigma}_{ij}(s, m^2, \mu_F^2, \mu_R^2) \tag{1}$$

where x_1 and x_2 are the fractional momenta carried by the colliding partons and f_i^p are the proton parton densities. The total partonic cross section has been completely calculated up to NLO [6, 7]. The partonic cross section is given by

$$\begin{aligned} \widehat{\sigma}_{ij}(s, m, \mu_F^2, \mu_R^2) &= \frac{\alpha_s^2(\mu_R^2)}{m^2} \left\{ f_{ij}^{(0,0)}(\rho) \right. \\ &+ \left. 4\pi\alpha_s(\mu_R^2) \left[f_{ij}^{(1,0)}(\rho) + f_{ij}^{(1,1)}(\rho) \ln\left(\frac{\mu_F^2}{m^2}\right) \right] + \mathcal{O}(\alpha_s^2) \right\} \end{aligned} \tag{2}$$

where $\rho = 4m^2/s$ and $f_{ij}^{(k,l)}$ are the scaling functions to NLO [6, 7]. At small ρ, the $\mathcal{O}(\alpha_s^2)$ and $\mathcal{O}(\alpha_s^3)$ $q\bar{q}$ and the $\mathcal{O}(\alpha_s^2)$ gg scaling functions become small while the $\mathcal{O}(\alpha_s^3)$ gg and qg scaling functions plateau at finite values. Thus, at collider energies, the total cross sections are primarily dependent on the small x parton densities and phase space. The total cross section does not depend on any kinematic variables, only on the quark mass, m, and the renormalization and factorization scales with central value $\mu_{R,F} = \mu_0 = m$.

2.2. Formation of quarkonia out of the two heavy quarks

The nonperturbative evolution of the $Q\bar{Q}$ pair into a quarkonium has been discussed extensively in terms of models and in terms of the language of effective theories of QCD [8, 9]. Different treatments of this evolution have led to various theoretical models for inclusive quarkonium production. Most notable among these are the color-singlet model (CSM), the color-evaporation model (CEM) and the non-relativistic QCD (NRQCD) factorization approach. In this review we will mainly discuss the NRQCD approach, as theoretically, it is the most modern and acceptable one. However, we will touch upon CSM and CEM briefly.

2.2.1. The color singlet model :

The CSM was first proposed shortly after the discovery of the J/ψ [10, 11, 12, 13]. In this model, it is assumed that the $Q\bar{Q}$ pair that evolves into the quarkonium is in a color-singlet state and that it has the same spin and angular-momentum quantum numbers as the quarkonium. In the CSM, the production rate

for each quarkonium state is related to the absolute values of the color-singlet $Q\bar{Q}$ wave function and its derivatives, evaluated at zero $Q\bar{Q}$ separation. These quantities can be extracted by comparing theoretical expressions for quarkonium decay rates in the CSM with experimental measurements. Once this extraction has been carried out, the CSM has no free parameters. The CSM was successful in predicting quarkonium production rates at relatively low energy [14]. Recently, it has been found that, at high energies, very large corrections to the CSM appear at next-to-leading order (NLO) and next-to-next-to-leading order (NNLO) in α_s [15, 16, 17]. Consequently, the possibility that the CSM might embody an important production mechanism at high energies has re-emerged. However, given the very large corrections at NLO and NNLO, it is not clear that the perturbative expansion in α_s is convergent. The NRQCD factorization approach encompasses the color-singlet model, but goes beyond it.

2.2.2. The color evaporation model:

The CEM [18, 19, 20] is motivated by the principle of quark-hadron duality. In the CEM, it is assumed that every produced $Q\overline{Q}$ pair evolves into a quarkonium if it has an invariant mass that is less than the threshold for producing a pair of open-flavor heavy mesons. It is further assumed that the nonperturbative probability for the $Q\overline{Q}$ pair to evolve into a quarkonium state H is given by a constant F_H that is energy-momentum and process independent. Once F_H has been fixed by comparison with the measured total cross section for the production of the quarkonium H, the CEM can predict, with no additional free parameters, the momentum distribution of the quarkonium production rate. The CEM predictions provide good descriptions of the CDF data for J/ψ, $\psi(2S)$, and χ_c production at $\sqrt{s} = 1.8$ TeV [20].

The heavy quark production cross section are calculated to NLO in pQCD using the CT10 parton densities [21]. The mass and scale parameters used for open and hidden heavy flavor production are obtained by fitting the energy dependence of open heavy flavor production to the measured total cross sections [22**?**]. Those obtained for open charm are $m_c = 1.27 \pm 0.09$ GeV, $\mu_F/m_{T\,c} = 2.10^{+2.55}_{-0.85}$, and $\mu_R/m_{T\,c} = 1.60^{+0.11}_{-0.12}$ [22]. The botttom quark mass and scale parameters are $m_b = 4.65 \pm 0.09$ GeV, $\mu_F/m_{T\,b} = 1.40^{+0.75}_{-0.47}$, and $\mu_R/m_{T\,b} = 1.10^{+0.26}_{-0.19}$ [**?**]. The quarkonium production cross sections are calculated in the color evaporation model with normalizations determined from fitting the scale parameter to the shape of the energy-dependent cross sections [22**?**]. The resulting uncertainty bands are smaller than those obtained with the fiducial parameters used in Ref. [23]. We note that the new results are within the uncertainties of those Ref. [23]. Indeed, the charm cross sections reported at the LHC agree better with the new values of the mass and scale than the central value of $m_c = 1.5$ GeV, $\mu_F/m_T = \mu_R/m_T = 1$.

Table 1: Heavy quark and quarkonia production cross sections at $\sqrt{s_{_{NN}}} = 2.76$ TeV. The cross sections are given per nucleon pair while $N^{\rm PbPb}$ gives the initial number of heavy quark pair/quarkonia per Pb+Pb event.

	$c\bar{c}$	J/ψ	$b\bar{b}$	Υ
σ_{pp}	$4.11^{+2.69}_{-2.50}$ mb	$21.6^{+10.6}_{-10.4}$ μb	$110.5^{+15.1}_{-14.2}$ μb	$0.22^{+0.07}_{-0.06}$ μb
$\sigma_{\rm PbPb}$	$3.21^{+2.1}_{-1.95}$ mb	$16.83^{+8.26}_{-8.10}$ μb	$100.5^{+13.7}_{-12.9}$ μb	$0.199^{+0.063}_{-0.054}$ μb
$N^{\rm PbPb}$	18.12^{+12}_{-11}	$0.0952^{+0.047}_{-0.046}$	$0.57^{+0.08}_{-0.07}$	$0.001123^{+0.0004}_{-0.0003}$

The central EPS09 NLO parameter set [24] is used to calculate the modifications of the parton distribution functions (nPDF) in Pb+Pb collisions, referred as cold nuclear matter (CNM) effects. The CNM uncertainty is calculated by adding the EPS09 NLO uncertainties in quadrature.The production cross sections for heavy flavor and quarkonia at $\sqrt{s_{_{NN}}}$ = 2.76 TeV [25] are given in Table 1. The yields in a minimum bias Pb+Pb event is obtained from the per nucleon cross section, $\sigma_{\rm PbPb}$, in Table 1, as

$$N = \frac{A^2 \sigma_{\rm PbPb}}{\sigma^{\rm tot}_{\rm PbPb}} \ . \tag{3}$$

At 2.76 TeV, the total Pb+Pb cross section, $\sigma^{\rm tot}_{\rm PbPb}$, is 7.65 b [26].

2.2.3. The NRQCD factorization approach:

Quantum Chromodynamics (QCD) describes the strong interaction among the quarks and gluons via perturbative calculations utilising its property called asymptotic freedom. On the other hand, these quarks and gluons are confined inside hadrons which are the colour singlet states. Confinement is a purely non-perturbative phenomenon which is not very well understood yet. The study of quarkonia ($Q\bar{Q}$) serves as an effective tool to look at both of these perturbative and non-perturbative aspects of QCD. The quarkonia states differ from most other hadrons due to the small velocity, v of the massive constituents and thus can be treated using non-relativistic formalism [27, 28]. In a simple picture, one can think of a quarkonium as a heavy quark pair ($Q\bar{Q}$) bound in a colour singlet state by some effective potential interaction, where the constituents are separated by distances much smaller than $1/\Lambda_{\rm QCD}$ where $\Lambda_{\rm QCD}$ is the QCD scale. This interaction gets screened in the presence of a deconfined medium like Quark Gluon Plasma (QGP), causing the bound state to melt away and thus the quarkonia yields are suppressed in the heavy ion collisions. This makes quarkonia an important probe of QGP. However cold nuclear matter effects such as modification of parton distribution functions of nucleons inside nucleus also affect their yields. There have been immense experimental [29, 30, 31, 32] and theoretical works [33, 34, 35, 36] on quarkonia modifications in PbPb collisions for which understanding of quarkonia production in pp collisions is an important prerequisite.

The massive quarks (with $m_c \sim 1.6$ GeV/c^2, $m_b \sim 4.5$ GeV/c^2) are produced in initial stages in hadronic collision with high momentum transfer and thus can be treated perturbatively [7]. The emergence of quarkonia out of the two massive quarks, on the other hand can only be described non-perturbatively using different models [8, 37]. The Colour Singlet Model (CSM) [10, 13], Colour Evaporation Model (CEM) [18, 19], the Fragmentation Scheme and the NRQCD factorisation formalism are some of the well established models for quarkonia production. In the framework of CSM, the $Q\bar{Q}$ pair, eventually evolving into the quarkonium, is assumed to be in Colour Singlet (CS) state and that has spin and angular momentum same as that of quarkonium. Apart from comprising of the CSM, the NRQCD factorisation approach incorporates the Colour Octet (CO) states as well.

In the formalism of the NRQCD factorisation approach, the evolution probability of $Q\bar{Q}$ pair into a state of quarkonium is expressed as matrix elements of NRQCD operators expanded in terms of heavy quark velocity v (for $v \ll 1$) [8]. The factorisation formulae were then used to calculate production cross-sections and decay rates of quarkonia states. The full structure of the $Q\bar{Q}$ Fock space is considered and spanned by $n{=}^{2s+1}L_J^{[a]}$ state where s is the spin, L is the orbital angular momentum, J is the total angular momentum and a (colour multiplicity) = 1 for CS and 8 for CO states. The produced CO states of $Q\bar{Q}$ pair at short distances emerge as CS quarkonia by emitting soft gluons non-perturbatively. The short distance cross-sections are obtained theoretically using methods of perturbative QCD (pQCD). The long distance matrix elements (LDME) that correspond to the probability of $Q\bar{Q}$ pair to emerge as quarkonium are extracted by fitting the measured cross-section data.

There have been several works on bottomonia production based on NRQCD formalism. In Ref. [38], a Monte Carlo framework has first been employed with CO mechanism for inclusive bottomonia production and few NRQCD CO matrix elements for Υ(1S) have been extracted at the Tevatron energy. The study has been extended to the whole Υ(nS) family in Ref. [39] to find CO matrix elements using CDF measurements at Tevatron. In Ref. [**?**] the CO matrix elements are obtained for Υ(nS) family and the feed downs from χ_b(1P) and χ_b(2P) to Υ(1S) have been considered. In Ref. [40], the Υ production has been obtained via S-wave CO states calculated at Next to Leading Order (NLO). The LDMEs are obtained by fitting the Tevatron data. The ratios of NLO to LO total cross-sections have been obtained at Tevatron and LHC energies. Polarisation of inclusive Υ has been obtained albeit with large uncertainties. In Ref. [41] both CS and CO states along with feed down contributions from higher states have been considered to study the quarkonia yields for RHIC and LHC energies. Using Collins-Soper-Sterman (CSS) formalism, an

extension of the NRQCD prediction has been carried forward for heavy quarkonium production at low p_T by considering soft gluon resummation at all orders in Ref. [42].

Both production and polarisation of Υ(nS) at NLO have been discussed in Ref. [43] within the framework of NRQCD. The CO matrix elements are obtained by fitting with experimental data. The study is updated in Ref. [44] by considering feed down from χ_{bJ}(mP) states in Υ(nS) production. The yields and polarisations of Υ(nS) measured at Tevatron and LHC are well explained by this work. The NLO study in Ref. [45] describes the yields and polarisations of Υ(nS) at LHC which includes feed down contributions from higher states. In Ref. [46], production cross-section for Υ(nS), χ_{bJ}, η_b and h_b have been calculated using NRQCD, as produced in hard photo production and fragmentation processes at LHC energies.

A LO NRQCD analyis is useful as it is straightforward and unique and once the parameters are obtained by fitting over large datasets it has excellent predictability power for unknown cross sections. The short distance QCD cross-sections calculation techniques at NLO are not unique. Moreover the different components of pQCD NLO cross sections are not available in public domain. Many NLO analysis do not include the feed down contribution from the higher states. It is shown that there is a large difference amoung the LDMEs obtained by different analysis at NLO. In this paper, the LO NRQCD calculations for the differential production cross-sections of Υ states in p+p collisions have been presented. The NRQCD formalism is described briefly in Section 2.2.3. A large set of data from Tevatron [47] and LHC [48, 49, 50, 51, 52] is used to extract the LDMEs required for the Υ production and then results are presented in Section 2.2.3. A comparison of the obtained LDMEs with the previous NRQCD studies both at LO and NLO has been made. The summary of our findings are discussed in Section 2.2.3. An updated QCD LO study on the bottomonia hadroproduction is useful as it provides a reference for comparison with NLO calculations.

Bottomonia production in p+p collisions. In order to study heavy quarkonium yield, the NRQCD framework serves as an efficient theoretical tool. The processes that govern the differential production of heavy mesons like bottomonium, as functions of p_T are mostly 2→2 operations. These processes can be denoted generically by $a+b \rightarrow \Upsilon + X$, where a and b are the incident light partons, Υ is the heavy meson and X is final state light parton. The double differential cross-section as a function of p_T and rapidity (y) of the heavy meson can be written as [54],

$$\begin{aligned} \frac{d^2\sigma^{\Upsilon}}{dp_T dy} &= \sum_{a,b} \int_{x_a^{min}}^{1} dx_a G_{a/p}(x_a, \mu_F^2) G_{b/p}(x_b, \mu_F^2) \\ &\times 2p_T \frac{x_a x_b}{x_a - \frac{m_T}{\sqrt{s}} e^y} \frac{d\sigma}{d\hat{t}} \end{aligned} \tag{4}$$

where, $G_{a/p}(G_{b/p})$ are the colliding parton $(a(b))$ distribution functions in the incident protons. They depend on the fractions $x_a(x_b)$, of the total momentum carried by the incident partons and the scale of factorisation μ_F. Here $\sqrt{s}$ represents the total center of mass energy of the pp system and m_T $(= \mu_F)$ stands for the transverse mass,

Table 2: Necessary and pertinent branching fractions for bottomonia family [45, 53].

Meson from	Meson to								
	Υ(3S)	χ_{b0}(2P)	χ_{b1}(2P)	χ_{b2}(2P)	Υ(2S)	χ_{b0}(1P)	χ_{b1}(1P)	χ_{b2}(1P)	Υ(1S)
χ_{b0}(3P)	0.005				0.002				0.002
χ_{b1}(3P)	0.104				0.037				0.038
χ_{b2}(3P)	0.061				0.019				0.019
Υ(3S)		0.131	0.126	0.059	0.199	0.003	0.0017	0.019	0.066
χ_{b0}(2P)					0.014				0.004
χ_{b1}(2P)					0.199				0.092
χ_{b2}(2P)					0.106				0.070
Υ(2S)						0.038	0.0715	0.069	0.260
χ_{b0}(1P)									0.019
χ_{b1}(1P)									0.352
χ_{b2}(1P)									0.180

Table 3: CS and CO elements for Υ family, obtained theoretically/extracted using experimental data [41, 44].

Direct Contributions	Feed down contributions from higher s-wave states	Feed down contributions from higher p-wave states
$M_L(b\bar{b}([^3S_1]_1) \to \Upsilon(3S))$ =4.3 GeV^3	$M_L(b\bar{b}([^3S_1]_1) \to \Upsilon(3S, 2S))$ =4.3, 4.5 GeV^3	$M_L(b\bar{b}([^3P_0]_1) \to \chi_{b0}(1P))$ =0.100m_b^2 GeV^3
$M_L(b\bar{b}([^3S_1]_1) \to \Upsilon(2S))$ =4.5 GeV^3	$M_L(b\bar{b}([^3S_1]_8) \to \Upsilon(3S, 2S))$	$M_L(b\bar{b}([^3S_1]_8) \to \chi_{b0}(1P))$ =0.0094 GeV^3
$M_L(b\bar{b}([^3S_1]_1) \to \Upsilon(1S))$ =10.9 GeV^3	$M_L(b\bar{b}([^1S_0]_8) \to \Upsilon(3S, 2S))$	$M_L(b\bar{b}([^3P_0]_1) \to \chi_{b0}(2P))$ =0.100m_b^2 GeV^3
$M_L(b\bar{b}([^3S_1]_8) \to \Upsilon(nS))$	$M_L(b\bar{b}([^3P_0]_8) \to \Upsilon(3S, 2S))$	$M_L(b\bar{b}([^3S_1]_8) \to \chi_{b0}(2P))$ =0.0109 GeV^3
$M_L(b\bar{b}([^1S_0]_8) \to \Upsilon(nS))$	$M_L(b\bar{b}([^3P_1]_8) \to \Upsilon(3S, 2S))$ =3$M_L(b\bar{b}([^3P_0]_8) \to \Upsilon(3S, 2S))$	$M_L(b\bar{b}([^3P_0]_1) \to \chi_{b0}(3P))$ =0.100m_b^2 GeV^3
$M_L(b\bar{b}([^3P_0]_8) \to \Upsilon(nS))$	$M_L(b\bar{b}([^3P_2]_8) \to \Upsilon(3S, 2S))$ =5$M_L(b\bar{b}([^3P_0]_8) \to \Upsilon(3S, 2S))$	$M_L(b\bar{b}([^3S_1]_8) \to \chi_{b0}(3P))$ =0.0069 GeV^3
$M_L(b\bar{b}([^3P_1]_8) \to \Upsilon(nS))$ 3$M_L(b\bar{b}([^3P_0]_8) \to \Upsilon(nS))$		
$M_L(b\bar{b}([^3P_2]_8) \to \Upsilon(nS))$ 5$M_L(b\bar{b}([^3P_0]_8) \to \Upsilon(nS))$		

$m_T^2 = p_T^2 + M^2$ of the quarkonium. The relation between x_a and x_b and the expression for x_a^{min} are given in our earlier work [54]. The $d\sigma/d\hat{t}$ in Eq. 4 is the parton level cross-section and is defined as [8],

$$\frac{d\sigma}{d\hat{t}} = \frac{d\sigma}{d\hat{t}}(ab \to Q\bar{Q}(^{2s+1}L_J) + X) M_L(Q\bar{Q}(^{2s+1}L_J) \to \Upsilon) \tag{5}$$

The first term in RHS is the short distance contribution, that corresponds to the $Q\bar{Q}$ pair production in specific colour and spin configuration and is calculable using perturbative QCD (pQCD) [**?** 55, 56, 57, 58, 59]. The other term in the RHS of Eq.(5) is the Long Distance Matrix Element (LDME) and refers to the probability of the $Q\bar{Q}$ state to convert into a quarkonium state. They are determined by contrasting with experimental observations.

The NRQCD formalism provides an adequate procedure to estimate a quantity as an expansion in heavy quark relative velocity, v inside $Q\bar{Q}$ bound state. The LDME in Eq.(5) do scale with definitive power in v. The quarkonium yield depends on the $^3S_1^{[1]}$ and $^3P_J^{[1]}$(J=0,1,2) CS states and $^1S_0^{[8]}$, $^3S_1^{[8]}$ and $^3P_J^{[8]}$ CO states in the limit $v \ll 1$. The superscripts in square brackets represent the colour structure of the bound state, 1 for the CS and 8 for the CO. The direct production cross-section for Υ in differential form can thus be expressed as the sum of all contributions,

$$\begin{aligned}
d\sigma(\Upsilon(nS)) &= d\sigma(Q\overline{Q}([^3S_1]_1)) M_L(Q\bar{Q}([^3S_1]_1) \to \Upsilon(nS)) \\
&+ d\sigma(Q\overline{Q}([^1S_0]_8)) M_L(Q\bar{Q}([^1S_0]_8) \to \Upsilon(nS)) \\
&+ d\sigma(Q\overline{Q}([^3S_1]_8)) M_L(Q\bar{Q}([^3S_1]_8) \to \Upsilon(nS)) \\
&+ d\sigma(Q\overline{Q}([^3P_0]_8)) M_L(Q\bar{Q}([^3P_0]_8) \to \Upsilon(nS)) \\
&+ d\sigma(Q\overline{Q}([^3P_1]_8)) M_L(Q\bar{Q}([^3P_1]_8) \to \Upsilon(nS)) \\
&+ d\sigma(Q\overline{Q}([^3P_2]_8)) M_L(Q\bar{Q}([^3P_2]_8) \to \Upsilon(nS)) \\
&+ ...
\end{aligned} \tag{6}$$

The dots include terms having contributions in higher powers of v.

The contributions from CS-$[^3P_J]_1$ and CO-$[^3S_1]_8$ states are in the same order of v for the p-wave bound states, $\chi_b(nP)$. The angular momentum barriers of the p-wave states are held responsible for that to happen and thereby making them important enough to be considered. The differential cross-section for χ_b production henceforth is given by,

$$\begin{aligned}
d\sigma(\chi_{bJ}(1P)) &= d\sigma(Q\overline{Q}([^3P_J]_1)) M_L(Q\bar{Q}([^3P_J]_1) \to \chi_{bJ}(1P)) \\
&+ d\sigma(Q\overline{Q}[^3S_1]_8)) M_L(Q\bar{Q}([^3S_1]_8) \to \chi_{bJ}(1P)) \\
&+ ...
\end{aligned} \tag{7}$$

The experimental observations of Υ production at LHC energies, not only have contributions from direct yield, but also consist of feed downs from decay of heavier bottomonia states. The corresponding branching fractions are provided in Table 2.

We require both CS and CO matrix elements in order to get theoretical predictions for the production of bottomonia at the Tevatron and LHC energies. The corresponding expressions and numerical values for CS states are obtained from Ref. [**?**]. The CO states, on the other hand, cannot be directly connected to the non-relativistic wavefunctions of heavy mesons, as these are associated with a higher Fock state. Experimentally measured data sets are therefore

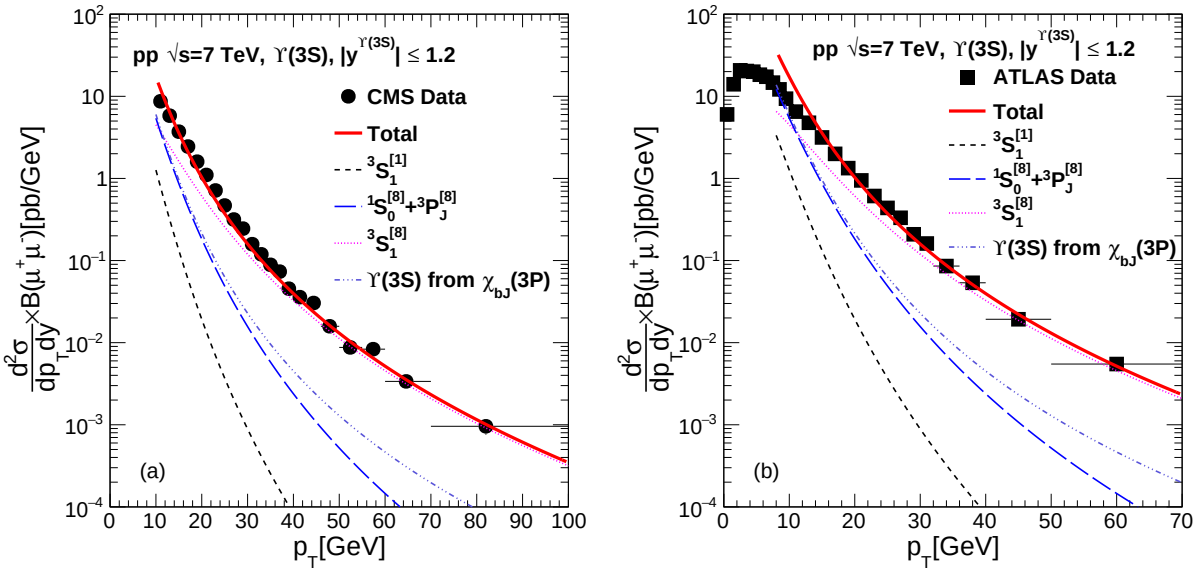

Figure 1: The NRQCD calculations of production cross-section of $\Upsilon(3S)$ in p+p collisions at $\sqrt{s}$ = 7 TeV in central rapidities, as a function of transverse momentum compared with the measured data at CMS [49] and ATLAS [50] experiment.

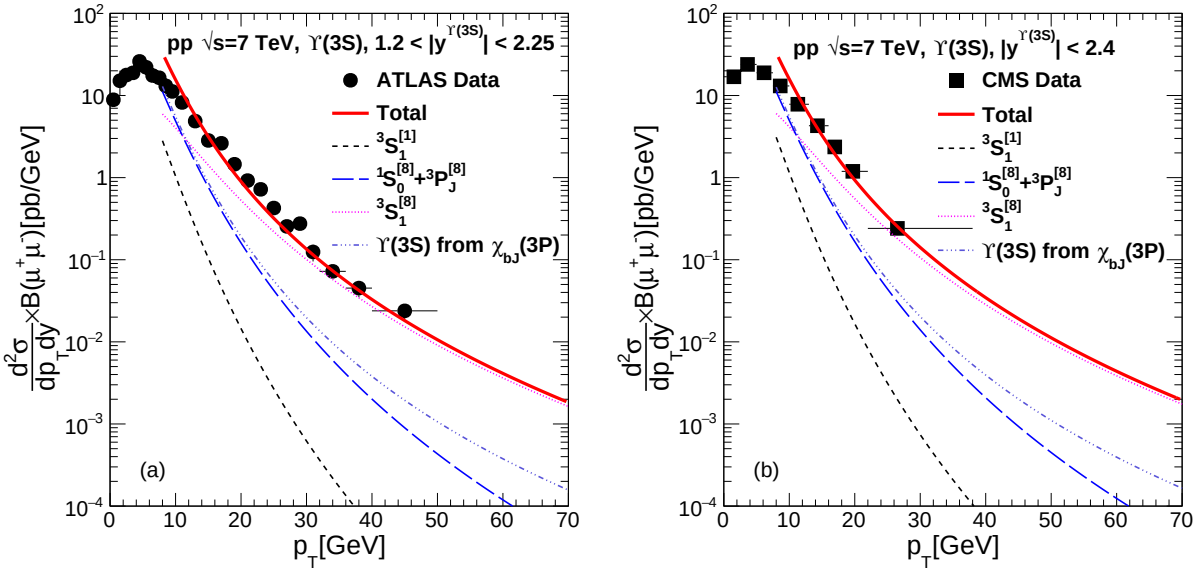

Figure 2: The NRQCD calculations of production cross-section of $\Upsilon(3S)$ in p+p collisions at $\sqrt{s}$ = 7 TeV in forward rapidities, as a function of transverse momentum compared with the measured data at ATLAS [50] and CMS [51] experiments.

employed to obtain them as in Refs. [**?** 58, 59]. The CS operators along with their theoretical values and the CO operators to be fitted are listed in Table 3, where, n=1,2,3. For the CO elements related to p-wave states, needed as the feed down contributions, we have used values obtained by Ref. [41, 44] for the present purpose. In our calculations, we have used CT18NLO parametrisation [60] for parton distribution functions and the bottom quark mass m_b is taken to be 4.88 GeV. The short distance cross-sections for $[^1S_0]_8$ and $[^3P_J]_8$ states having similar p_T dependencies, the corresponding distributions become sensitive upto a linear combination of their LDMEs. We therefore take resort to a linear combination following Ref. [54] as,

Table 4: Comparison of CS elements and CO LDMEs extracted from fitting with experimental data using NRQCD formalism for Υ(3S).

Ref. (LO/NLO)	PDF	m_b (GeV)	$M_L(b\bar{b}([^3S_1]_1 \rightarrow \Upsilon(3S)$ (GeV^3)	$M_L(b\bar{b}([^3S_1]_8 \rightarrow \Upsilon(3S)$ (GeV^3)	$M_L(b\bar{b}([^1S_0]_8, [^3P_0]_8 \rightarrow \Upsilon(3S)$ (GeV^3)	p_T-cut GeV/c
present (LO)	CT18	4.88	4.3	0.0543±0.0007	0.0097±0.0005	8
[39] (LO)	CTEQ4L	4.88	3.54	0.099±0.011	0	2
				0.091±0.015	0	4
				0.068±0.011	0	8
[**?**] (LO)	CTEQ5L	4.77	4.3±0.9	0.036±0.019	0.0108±0.0086	8
				0.039±0.017	0.0342±0.0276	
	MRSTLO	4.77	4.3±0.9	0.037±0.021	0.0150±0.0098	8
				0.041±0.019	0.0474±0.0312	
[40] (NLO)	CTEQ6M	5.18	1.128	0.03250±0.00876	0.000920±0.000968	-
[41] (LO)	MSTW08LO	4.88	4.3	0.0513±0.0085	0.0002±0.0062	-
[43] (NLO)	CTEQ6M	5.18	1.128	0.0271±0.0013	0.00956±0.00476	8
[44] (NLO)	CTEQ6M	5.18	1.128	0.0132±0.0020	-0.00520±0.00518	8

$$M_L(b\bar{b}([^1S_0]_8, [^3P_0]_8) \rightarrow \Upsilon(nS)) = \frac{M_L(b\bar{b}([^1S_0]_8) \rightarrow \Upsilon(nS))}{5} + \frac{3M_L(b\bar{b}([^3P_0]_8) \rightarrow \Upsilon(nS))}{m_b^2}.$$

Results and discussions. We first start with the production of Υ(3S) which has feed down contributions only from χ_b(3P). As described, the expressions and the values for the colour-singlet elements can be obtained by solving the non-relativistic wavefunctions [58]. The CO LDMEs on the other hand, cannot be connected to the non-relativistic wavefunctions of $b\bar{b}$. The measured data sets from different experimental collaborations are thus used to constrain them.

Figure 1 shows the NRQCD calculations of production cross-section of Υ(3S) in p+p collisions as a function of transverse momentum compared with the measured data in CMS [49] and ATLAS [50] detectors at LHC in central rapidities. In Figure 2, similar comparisons have been shown with data for $1.2 < |y| < 2.25$ and $|y| < 2.4$ measured at ATLAS [50] and CMS [51] detectors respectively. Figure 3 corresponds to CMS [52] measurements at $\sqrt{s} = 13$ TeV for rapidities, $|y| < 0.6$, $0.6 < |y| < 1.2$ and $|y| < 1.2$, whereas in Figure 4 we have used measurements from CDF [47] collaboration in p +$\bar{\text{p}}$ at $\sqrt{s} = 1.8$ TeV with $|y| < 0.4$ as well as that from LHCb [48] collaboration in p+p

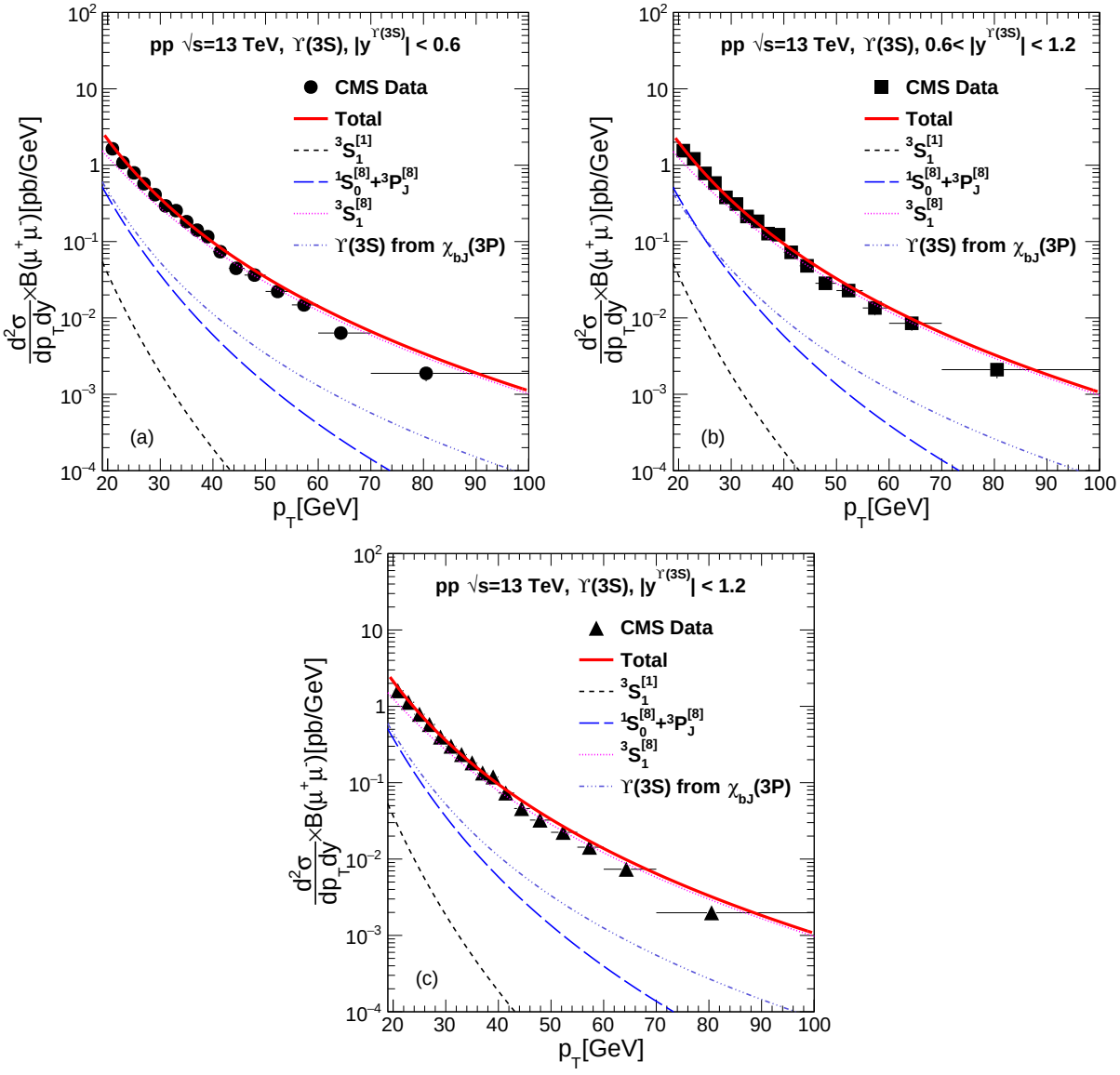

Figure 3: The NRQCD calculations of production cross-section of $\Upsilon(3S)$ in p+p collisions at $\sqrt{s}$ = 13 TeV in central and forward rapidities, as a function of transverse momentum compared with the measured data at CMS [52] experiment.

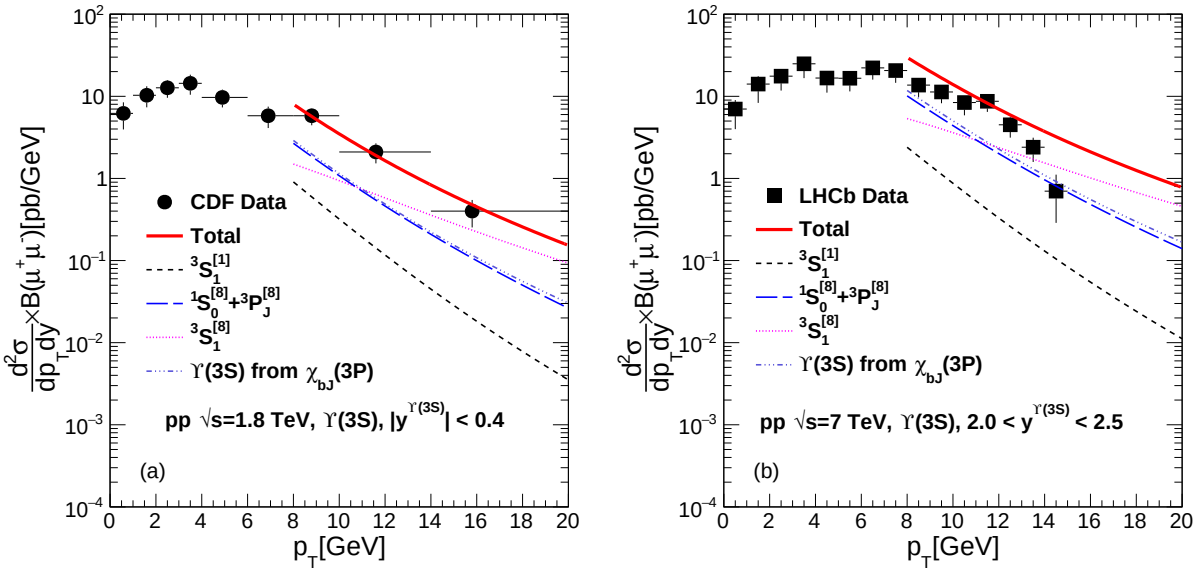

Figure 4: The NRQCD calculations of production cross-section of $\Upsilon(3S)$ in p +$\bar{\text{p}}$ collisions at $\sqrt{s}$ = 1.8 TeV and p+p collisions at 7 TeV in forward rapidities, as a function of transverse momentum compared with the measured data at CDF [47] and LHCb [48] experiment.

collisions at $\sqrt{s} = 7$ TeV with rapidities $2.0 < y < 2.5$. The LDMEs are obtained by a combined fit using all the aforesaid datasets. The χ^2/ndof is ~ 4 for the combined fitting.

Table 4 contains LDMEs for $\Upsilon(3S)$ extracted in present analysis in comparison with different other results. Our result for the matrix element $M_L(b\bar{b}([^3S_1]_8))$ shows a close proximity with LO analysis of Ref. [**?** 41], the errors being improved considerably. In our work, we have considered a linear combination of the other two colour octet LDMEs in the form of $\frac{M_L([^1S_0]_8)}{5} + \frac{3M_L([^3P_0]_8)}{m_b^2}$, same as that done in Ref. [41]. There have been different ways to treat the colour octet LDMEs in the literature. In Ref. [39], the authors have taken this combination as $M_L([^1S_0]_8) + \frac{5M_L([^3P_0]_8)}{m_b^2}$. In Ref. [**?**], these two matrix elements, $M_L([^1S_0]_8)$ and $\frac{5M_L([^3P_0]_8)}{m_b^2}$ have been extracted separately using two different PDFs. In each case however, they have extracted either of the two parameters considering the other to be vanishing. The work in Ref. [40] concentrates only on S-wave colour states. In Refs. [43, 44], the parameters, $M_L([^1S_0]_8)$ and $\frac{M_L([^3P_0]_8)}{m_b^2}$ have been extracted separately altogether. On the other hand in Ref. [45], the authors have considered different combinations of colour octet states to fit with the experimental data with NRQCD at LO and NLO using CTEQ6L1 and CTEQ6M PDFs respectively with m_b=4.75 GeV and $[^3S_1]_1$=3.54 GeV^3. Their extracted parameters are,

$$\begin{aligned} M_{0,r_0} &= [^1S_0]_8 + \frac{r_0}{m_b^2}[^3P_0]_8 = 0.0283 \pm 0.0007 \text{ GeV}^3 \\ M_{1,r_1} &= [^3S_1]_8 + \frac{r_1}{m_b^2}[^3P_0]_8 = 0.0083 \pm 0.0002 \text{ GeV}^3 \end{aligned} \tag{8}$$

with r_0=3.8 and r_1=-0.52 GeV^2.

After fixing the $\Upsilon(3S)$ yield, we next consider $\Upsilon(2S)$ production that has feed down contributions from $\Upsilon(3S)$, $\chi_b(2P)$ and $\chi_b(2P)$ states along with the direct production. The corresponding branching fractions for the feed down sectors are given in Table 2. We have used our extracted values of the $\Upsilon(3S)$ LDMEs for the feed down contributions

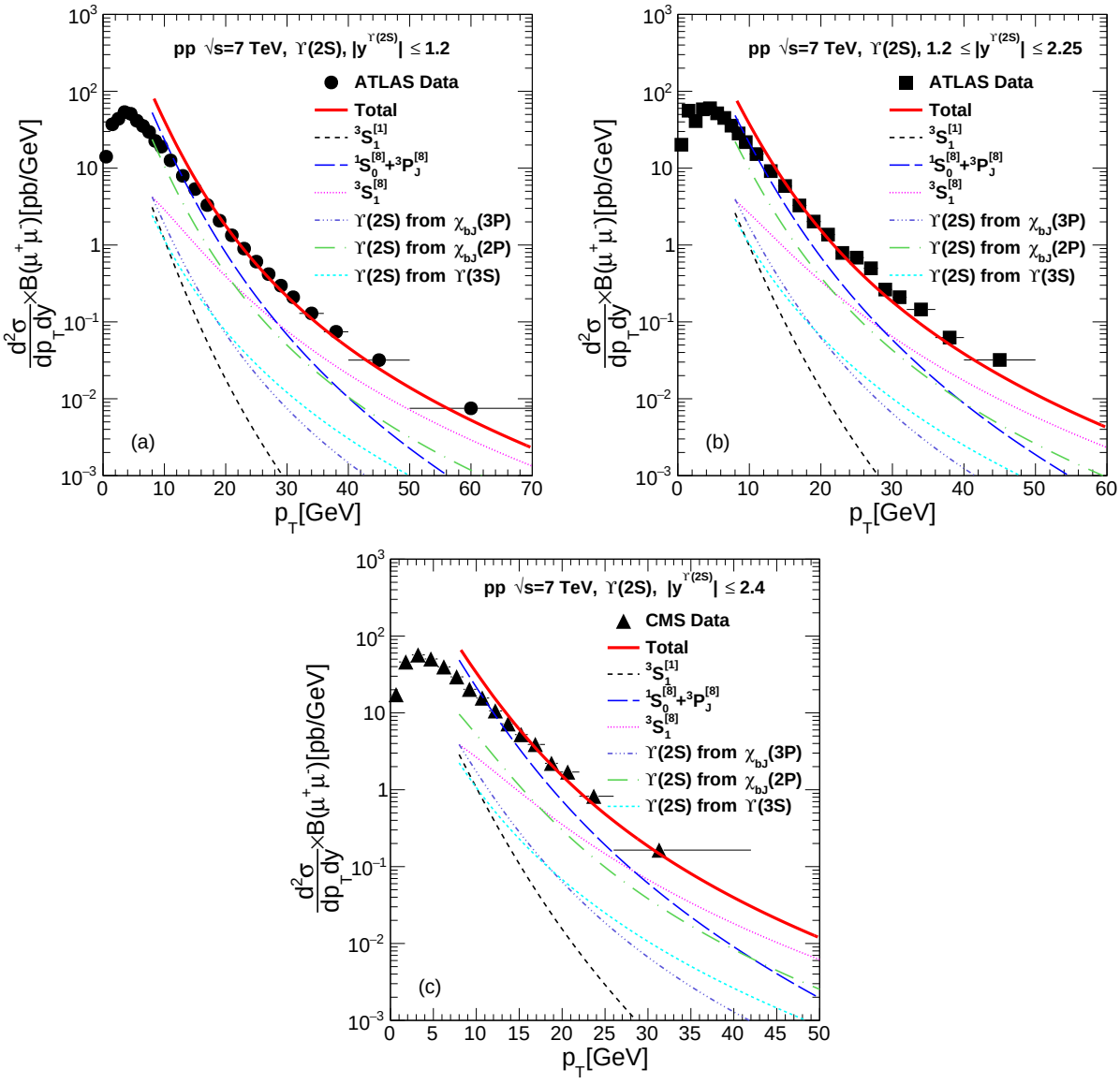

Figure 5: The NRQCD calculations of production cross-section of Υ(2S) in p+p collisions at $\sqrt{s}$ = 7 TeV in central and forward rapidities, as a function of transverse momentum compared with the measured data at CMS [51] and ATLAS [50] experiments.

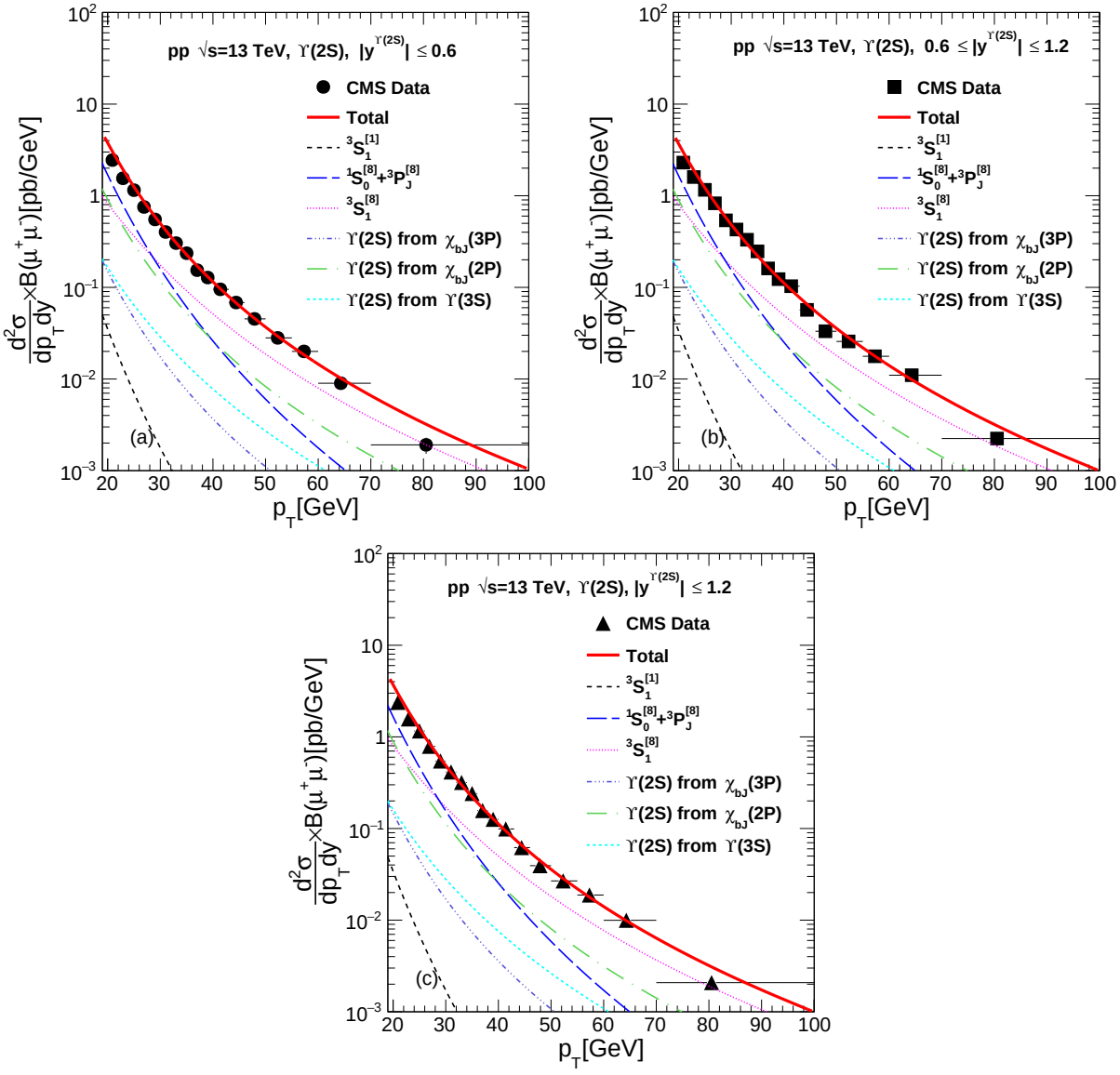

Figure 6: The NRQCD calculations of production cross-section of $\Upsilon(2S)$ in p+p collisions at $\sqrt{s}$ = 13 TeV in central and forward rapidities, as a function of transverse momentum compared with the measured data at CMS [52] experiment.

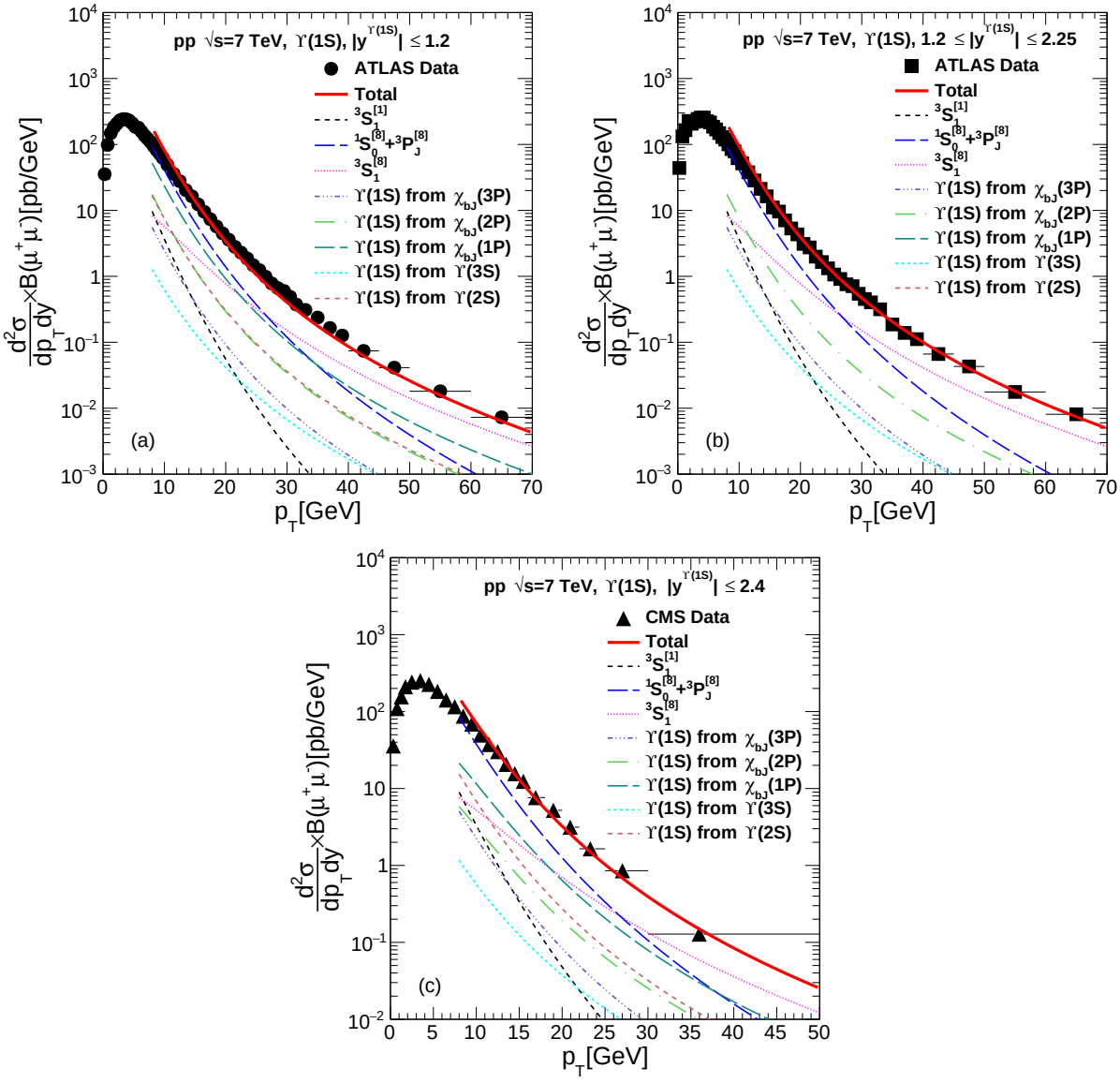

Figure 7: The NRQCD calculations of production cross-section of $\Upsilon(1S)$ in p+p collisions at $\sqrt{s}$ = 7 TeV in central and forward rapidities, as a function of transverse momentum compared with the measured data at ATLAS [50] and CMS [51] experiments.

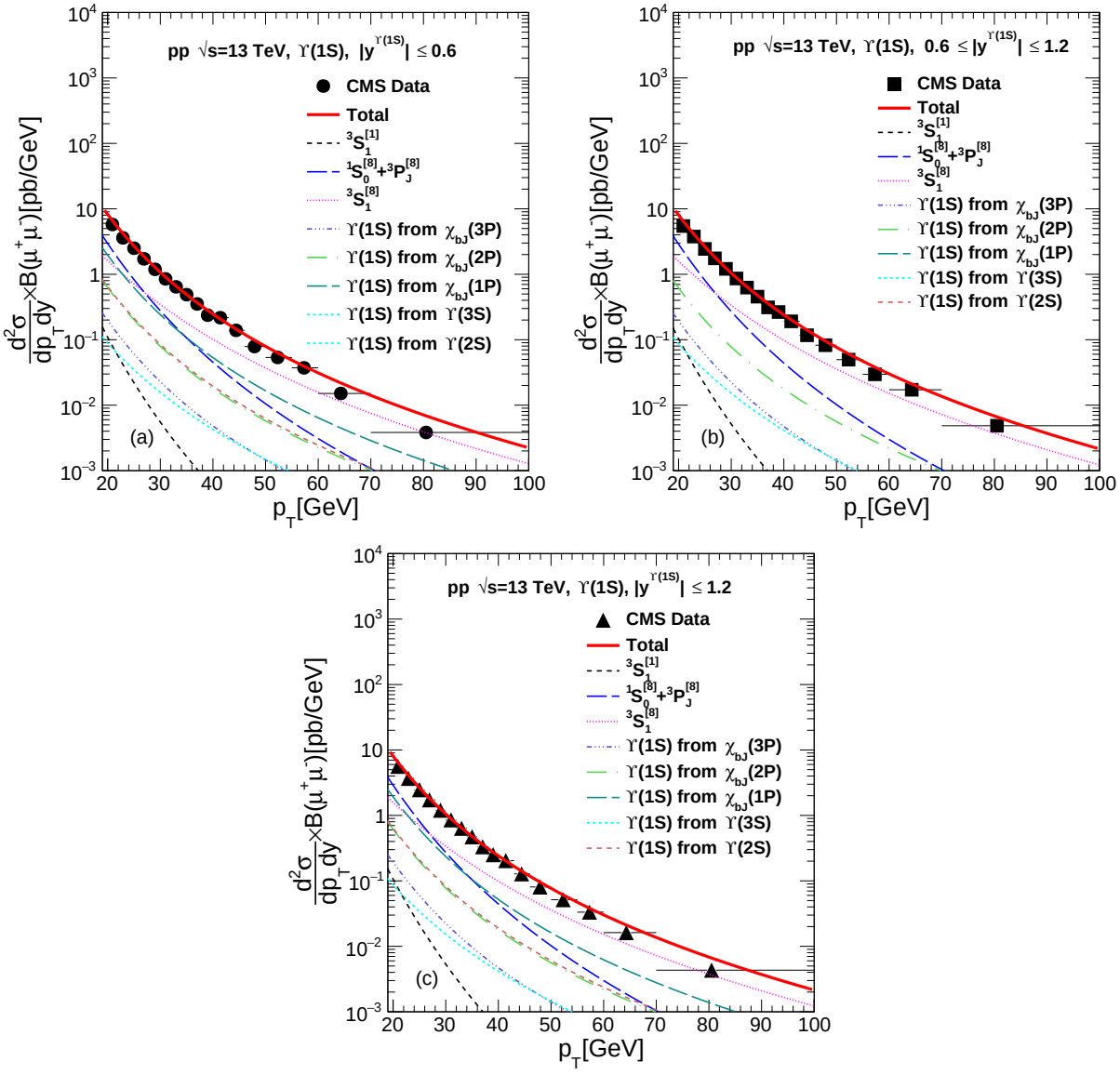

Figure 8: The NRQCD calculations of production cross-section of $\Upsilon(1S)$ in p+p collisions at $\sqrt{s}$ = 13 TeV in central and forward rapidities, as a function of transverse momentum compared with the measured data at CMS [52] experiment.

Table 5: Comparison of CS elements and CO LDMEs extracted from fitting with experimental data using NRQCD formalism for Υ(2S).

Ref. (LO/NLO)	PDF	m_b (GeV)	$M_L(b\bar{b}([^3S_1]_1 \to \Upsilon(2S)$ (GeV^3)	$M_L(b\bar{b}([^3S_1]_8 \to \Upsilon(2S)$ (GeV^3)	$M_L(b\bar{b}([^1S_0]_8, [^3P_0]_8 \to \Upsilon(2S)$ (GeV^3)	p_T-cut GeV/c
present (LO)	CT18	4.88	4.5	0.0391±0.0016	0.0477±0.0019	8
[39] (LO)	CTEQ4L	4.88	5.01	0.040±0.029	0	2
				0.073±0.018	0	4
				0.103±0.027	0	8
[**?**] (LO)	CTEQ5L	4.77	5.0±0.7	0.180±0.056	-0.102±0.097	8
				0.172±0.050	-0.106±0.102	
	MRSTLO	4.77	5.0±0.7	0.196±0.063	-0.087±0.111	8
				0.190±0.056	-0.089±0.117	
[41] (LO)	MSTW08LO	4.88	4.5	0.0224±0.0200	-0.0067±0.0084	-
[43] (NLO)	CTEQ6M	5.01	4.63	0.0030±0.0078	0.0075±0.0217	8
[44] (NLO)	CTEQ6M	5.01	4.63	0.0222±0.0024	-0.0003±0.0203	8

from the Υ(3S). To include the $\chi_b(nP)$ states feed down LDMEs are obtained from Ref. [41, 44].

In Fig 5, we have shown our NRQCD predictions of production cross-sections for Υ(2S) in p+p collisions as functions of p_T along with the measured data in CMS [51] and ATLAS [50] detectors at central and forward rapidities. All the contributions alongwith feed down ones are displayed separately. Fig. 6 describes the same alongwith the data from CMS detector at 13 TeV for both central and forward rapidities. Our results of CO LDMEs for Υ(2S) have been given in Table 5 along with existing results from different other groups. Our value for $M_L(b\bar{b}([^3S_1]_8 \to \Upsilon(2S))$ is in agreement with the values from other groups also $M_L(b\bar{b}([^1S_0]_8, [^3P_0]_8 \to \Upsilon(2S))$ does not have negative value (which is unphysical) unlike some other groups. The inclusion of 13 TeV data along with the incorporation of feed down from χ_b(3P), is expected to give better constrains of LDMEs.

In [39**?** , 41, 43, 44, 45], authors have considered different combinations of CO LDMEs that has already been described. In Ref. [45], the extracted parameters for Υ(2S) are,

$$M_{0,r_0} = 0.0607 \pm 0.0108 \text{ GeV}^3$$
$$M_{1,r_1} = 0.0108 \pm 0.0020 \text{ GeV}^3$$

with $[3S_1]_1$=4.63 GeV^3 and the values of r_0 and r_1 are same as given before. The χ^2/ndof for the combined fit in our analysis is $\sim$ 2.7.

Having completed Υ(3S) and Υ(2S) parts, we now move on to explore Υ(1S). Alongwith the direct yield, it has feed down contributions from higher S-wave states like Υ(3S) and Υ(2S), as well as P-wave states like χ_b(3P),

Table 6: Comparison of CS elements and CO LDMEs extracted from fitting with experimental data using NRQCD formalism for Υ(1S).

Ref. (LO/NLO)	PDF	m_b (GeV)	$M_L(b\bar{b}([^3S_1]_1 \rightarrow \Upsilon(1S)$ (GeV^3)	$M_L(b\bar{b}([^3S_1]_8 \rightarrow \Upsilon(1S)$ (GeV^3)	$M_L(b\bar{b}([^1S_0]_8, [^3P_0]_8 \rightarrow \Upsilon(1S)$ (GeV^3)	p_T-cut GeV/c
present (LO)	CT18	4.88	10.9	0.0601±0.0017	0.0647±0.0016	8
[39] (LO)	CTEQ4L	4.88	11.1	0.077±0.017	0	2
				0.087±0.016	0	4
				0.106±0.013	0	8
[**?**] (LO)	CTEQ5L	4.77	12.8±1.6	0.116±0.027	0.109±0.062	8
				0.124±0.025	0.111±0.065	
	MRSTLO	4.77	12.8±1.6	0.117±0.030	0.181±0.072	8
				0.130±0.028	0.186±0.075	
[41] (LO)	MSTW08LO	4.88	10.9	0.0477±0.0334	0.0121±0.0400	-
[43] (NLO)	CTEQ6M	4.75	9.282	-0.0041±0.0024	0.0780±0.0043	8
[44] (NLO)	CTEQ6M	PDG	9.282	0.0061±0.0024	0.0895±0.0248	8

χ_b(2P) and χ_b(1P). The associated branching functions are provided in Table 2. The extracted CO-LDMEs for Υ(3S) and Υ(2S) are used for feed down contributions, whereas the LDMEs for the χ_b(nP) states have been taken from Ref. [41, 44] for this present case study. In Fig. 7, we have displayed our NRQCD calculation of production cross-section of Υ(1S) as function of p_T along with the experimental measurements by ATLAS and CMS at $\sqrt{s}$=7 TeV in central rapidities. Finally in Fig. 8, we present our results along with the CMS measurements at 13 TeV with all the components separately to signify their relative contributions.

Table 6 shows our results for Υ(1S) parameters along with the results from different groups. The individual values of LDMEs are in agreement with the values from previous works but with considerable reduction in errors upon inclusion of 13 TeV data sets from CMS. The values of the parameters M_{0,r_0} and M_{1,r_1} extracted in Ref. [45] are,

$$M_{0,r_0} = 0.1370 \pm 0.0111\,\mathrm{GeV}^3,$$
$$M_{1,r_1} = 0.0117 \pm 0.0002\,\mathrm{GeV}^3$$

with $[3S_1]_1$=9.28 GeV^3 keeping r_0 and r_1 same as given before.

Summary. We have presented NRQCD calculations for the differential production cross-sections of Υ states in p+p collisions. Measured transverse momentum distributions of Υ(3S), Υ(2S) and Υ(1S) in p +$\bar{\mathrm{p}}$ collisions at $\sqrt{s}$ = 1.8 TeV and in p+p collisions at 7 TeV and 13 TeV are used to constrain the LDMEs. All the relevant feeddown contributions from higher mass states including the χ_b(3P) are taken in to account. The calculations for Υ(3S), Υ(2S)

and Υ(1S) are compared with the measured data at Tevatron and LHC. The formalism provides very good description of the data in large transverse momentum range at different collision energy. We compare the LDMEs for bottomonia obtained in this analysis with the results from earlier works. At high p_T, the colour singlet contribution is very small and LHC data in large p_T range help to constrain the relative contributions of different colour octet contributions. For Υ states at high p_T, the contribution of the $M_L(b\bar{b}([^3S_1]_8 \to \Upsilon(nS)))$ is highest which is opposite to the charmonia case where the contribution for the combination of $M_L(c\bar{c}([^1S_0]_8, [^3P_0]_8) \to \psi)$ is more [54]. In summary, we present a comprehensive lowest-order analysis of hadroproduction data of bottomonia states using the latest parton distribution functions and including very recent LHC data. The feed-down contributions from all the χ_b states are included in the calculations. The values of relevant LDMEs are extracted by doing a simultaneous fit of all the data sets. These values will be useful for predictions of quarkonia cross-section and for the purpose of a comparison with those obtained using the NLO formulations.

3. Bottomonia production mechanism in heavy ion collisions

3.1. Theory overview

3.1.1. Sequential suppression and lattice QCD

This subsection will include the details of the model by Strickland et. al. This reference have most of the details about the model [61]

3.1.2. Effect of nuclear PDFs on quarkonium production in nucleus–nucleus collisions

This subsection will include the details of the models which use nuclear PDFs for quarkonia production like EPS19 or Color Glass Condensate modes. etc. []. These effects are small for the Upsilon sector.

3.1.3. Collisional dissociation of quarkonia from final-state interactions

Modification of quarkonia in the presence of QGP. In the kinetic approach [62], the proper time τ evolution of the quarkonia population N_Q is given by the rate equation

$$\frac{dN_Q}{d\tau} = -\lambda_D \rho_g N_Q + \lambda_F \frac{N_{q\bar{q}}^2}{V(\tau)}, \tag{9}$$

where $V(\tau)$ is the volume of the deconfined spatial region and $N_{q\bar{q}}$ is the number of initial heavy quark pairs produced per event depending on the centrality defined by the number of participants $N_{\rm part}$. The λ_D is the dissociation rate obtained by the dissociation cross section averaged over the momentum distribution of gluons and λ_F is the formation rate obtained by the formation cross section averaged over the momentum distribution of heavy quark pair q and $\bar{q}$. ρ_g is the density of thermal gluons. The number of quarkonia at freeze-out time τ_f is given by the solution of Eq. (9),

$$N_Q(p_T) = S(p_T)\, N_Q^{\rm PbPb}(p_T) + N_Q^F(p_T). \tag{10}$$

Here $N_Q^{\rm PbPb}(p_T)$ is the number of initially-produced quarkonia (including shadowing) as a function of p_T and $S(p_T)$ is their survival probability from gluon collisions at freeze-out,

$$S(p_T) = \exp\left(-\int_{\tau_0}^{\tau_f} f(\tau)\lambda_{\rm D}(T, p_T)\, \rho_g(T)\, d\tau\right). \tag{11}$$

The temperature $T(\tau)$ and the QGP fraction $f(\tau)$ evolve from initial time τ_0 to freeze-out time τ_f due to expansion of the QGP. The initial temperature and the evolution is dependent on collision centrality $N_{\rm part}$. $N_Q^F(p_T)$ is the number of regenerated quarkonia per event,

$$N_Q^F(p_T) = S(p_T) N_{q\bar{q}}^2 \int_{\tau_0}^{\tau_f} \frac{\lambda_{\rm F}(T, p_T)}{V(\tau)\, S(\tau, p_T)} d\tau. \tag{12}$$

The nuclear modification factor (R_{AA}) can be written as

$$R_{AA}(p_T) = S(p_T)\, R(p_T) + \frac{N_Q^F(p_T)}{N_Q^{pp}(p_T)}. \tag{13}$$

Here $R(p_T)$ is the shadowing factor. R_{AA} as a function of collision centrality, including regeneration, is

$$R_{AA}(N_{\rm part}) = \frac{\int_{p_T\,\rm cut} N_Q^{pp}(p_T) S(p_T)\, R(p_T) dp_T}{\int_{p_T\,\rm cut} N_Q^{pp}(p_T) dp_T} + \frac{\int_{p_T\,\rm cut} N_Q^F(p_T) dp_T}{\int_{p_T\,\rm cut} N_Q^{pp}(p_T) dp_T} \tag{14}$$

Here $p_{T\ \rm cut}$ defines the p_T range for a given experimental acceptance. $N_Q^{pp}(p_T)$ is the unmodified p_T distribution of quarkonia obtained by NLO calculations and scaled to a particular centrality of the Pb+Pb collisions.

The evolution of the system for each centrality bin is governed by an isentropic cylindrical expansion with volume element

$$V(\tau) = \tau\, \pi\, (R + \frac{1}{2} a_T\, \tau^2)^2, \tag{15}$$

where $a_T = 0.1\, c^2$ fm^{-1} is the transverse acceleration [63]. The initial transverse size, R, as a function of centrality is

$$R(N_{\rm part}) = R_{0-5\%} \sqrt{\frac{N_{\rm part}}{(N_{\rm part})_{0-5\%}}}, \tag{16}$$

where $R_{0-5\%} = 0.96\, R_{\rm Pb}$ and $R_{\rm Pb}$ is the radius of the lead nucleus. The evolution of entropy density for each centrality is obtained by entropy conservation, $s(T)\, V(\tau) = s(T_0)\, V(\tau_0)$. The equation of state (EOS) obtained from Lattice QCD, along with a hadronic resonance gas, [64] is used to obtain the temperature as a function of proper time τ. The initial entropy density for each centrality is calculated using

$$s(\tau_0) = s(\tau_0)|_{0-5\%} \left(\frac{dN/d\eta}{N_{\rm part}/2}\right) \left(\frac{dN/d\eta}{N_{\rm part}/2}\right)^{-1}_{0-5\%}. \tag{17}$$

Measured values of $(dN/d\eta)/(N_{\rm part}/2)$ as a function of $N_{\rm part}$ [65, 66] are used in the calculations. The initial entropy density, $s(\tau_0)|_{0-5\%}$, for 0-5% centrality is

$$s(\tau_0)|_{0-5\%} = \frac{a_m}{V(\tau_0)|_{0-5\%}} \left(\frac{dN}{d\eta}\right)_{0-5\%}. \tag{18}$$

Here a_m (= 5) is a constant which relates the total entropy to the total multiplicity $dN/d\eta$. It is obtained from hydrodynamic calculations [67]. We estimate the initial temperature, T_0, in the 0-5% most central collisions from the total multiplictity in the rapidity region of interest, assuming that the initial time is $\tau_0 = 0.3$ fm/c over all rapidity. The total multiplicity in a given rapidity region is 3/2 times the charged particle multiplicity in Pb+Pb collisions at 2.76 TeV. With the lattice EOS, at midrapidity, with $(dN_{\rm ch}/d\eta)_{0-5\%} = 1600$ [65, 66], we find $T_0 = 0.484$ GeV. Likewise, at forward rapiidity, $2.5 \le y \le 4$ [68], $T_0 = 0.427$ GeV. The (proper) time evolution of temperature is shown in Fig. 9(a) and that of QGP fraction in Fig. 9(b), in the case of the most central (0-5%) collisions. Here we

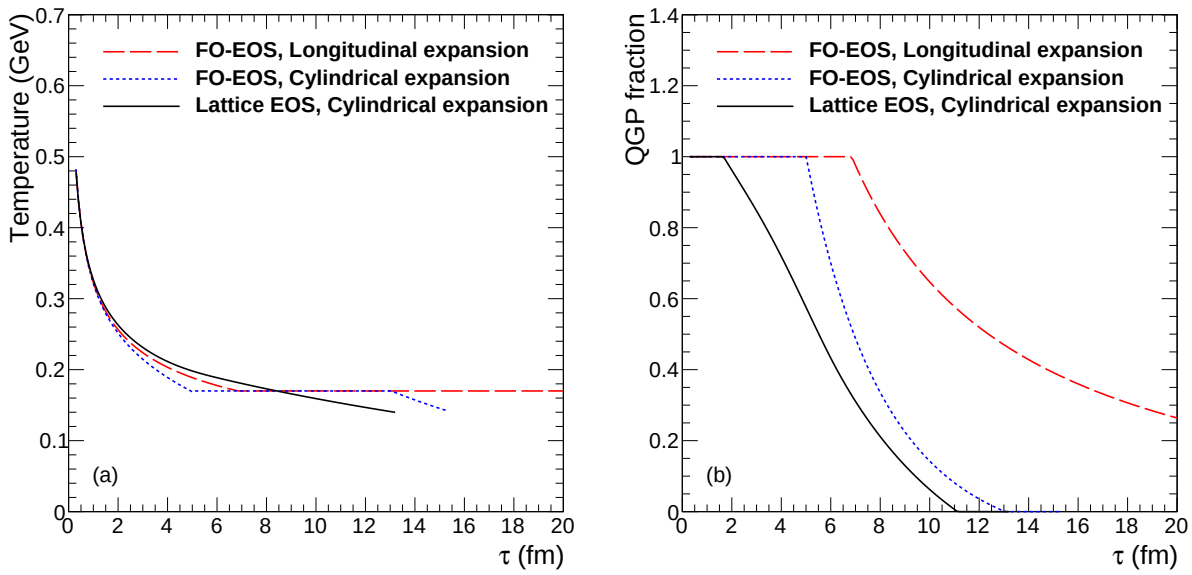

Figure 9: (Color online) (a) Temperature and (b) QGP fraction in the system as a function of proper time τ in case of the most central (0-5%) collisions for longitudinal and cylindrical expansions using first order and lattice equation of state.

compare the evolution obtained with longitudinal and cylindrical expansions using both a first order and the lattice EOS. For the first order EOS, T_c = 0.170 GeV. The QGP fraction goes from 1 to 0 at T_c assuming a mixed phase of QGP and hadrons. The QGP fraction in case of lattice EOS governs the number of degrees of freedom, decided by the entropy density. It is fixed to unity above an entropy density corresponding to a 2-flavour QGP and fixed to zero below entropy density for a hot resonance gas. The freeze out temperature in all cases is $T_f = 0.140$ GeV.

3.2. Dissociation Rate

In the color dipole approximation, the gluon dissociation cross section as function of gluon energy, q^0, in the quarkonium rest frame is [69]

$$\sigma_D(q^0) = \frac{8\pi}{3}\,\frac{16^2}{3^2}\,\frac{a_0}{m_q}\,\frac{(q^0/\epsilon_0 - 1)^{3/2}}{(q^0/\epsilon_0)^5}, \tag{19}$$

where ϵ_0 is the quarkonia binding energy and m_q is the charm/bottom quark mass and $a_0 = 1/\sqrt{m_q \epsilon_0}$. The values of ϵ_0 are taken as 0.64 and 1.10 GeV for the ground states, J/ψ and Υ(1S), respectively [70]. For the first excited state of bottomonia, Υ(2S), we use dissociation cross section from Ref. [71].

Figure 10 shows the gluon dissociation cross sections of J/ψ and Υ(1S) as a function of gluon energy. The dissociation cross section is zero when the gluon energy is less than the binding energy of the quarkonia. It increases with gluon energy and reaches a maximum at 1.2 (1.5) GeV for J/ψ (Υ(1S)). At higher gluon energies, the interaction probability decreases. The gluon energy q^0 is related to the square of the center of mass energy s, of the quarkonium-gluon system by

$$q^0 = \frac{s - M_Q^2}{2\,M_Q} \tag{20}$$

where $s = M_Q^2 + 2p_g\sqrt{M_Q^2 + p^2} - 2p_g\,p\cos\theta$, and M_Q and p are mass and momentum of quarkonium and θ is angle between the quarkonium and the gluon. We calculate the dissociation rate as a function of quarkonium momentum

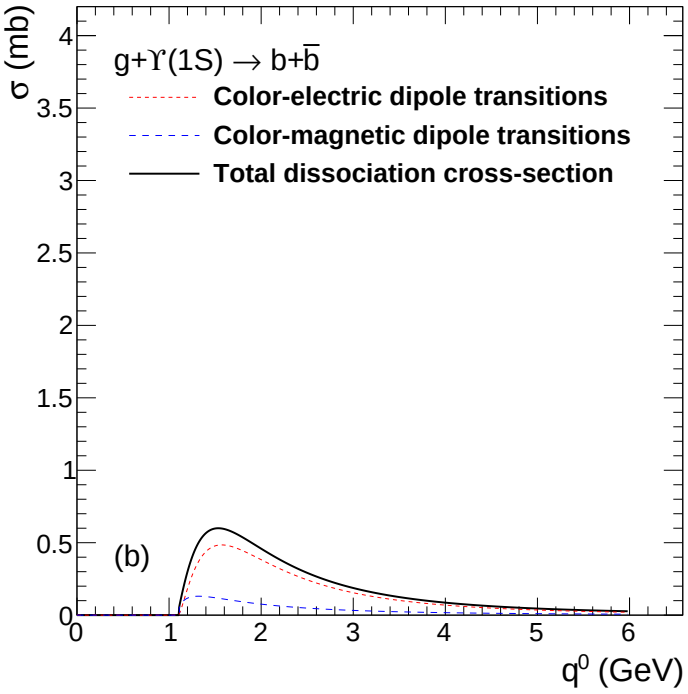

Figure 10: (Color online) Gluon dissociation cross section of quarkonia as a function of gluon energy (q^0) in quarkonia rest frame.

by integrating the dissociation cross section over thermal gluon momentum distribution $f_g(p_g)$,

$$\begin{aligned}\lambda_D \rho_g &= \langle \sigma v_{\rm rel} \rangle \, \rho_g = \frac{g_g}{(2\pi)^3} \int d^3p_g \, f_g(p_g) \, \sigma_D(s) v_{\rm rel}(s) \\ &= \frac{g_g}{(2\pi)^3} \int dp_g 2\pi p_g^2 f_g(p_g) \int d\cos\theta \, \sigma_D(s) \, v_{\rm rel}(s),\end{aligned} \tag{21}$$

where $\sigma_D(s) = \sigma_D(q^0(s))$. The relative velocity, $v_{\rm rel}$, between the quarkonium and the gluon is

$$v_{\rm rel} = \frac{s - M_Q^2}{2p_g\sqrt{M_Q^2 + p^2}}. \tag{22}$$

The J/ψ gluon dissociation rates as a function of T are shown in Fig. 11(a) and as a function of p_T in Fig. 11(b). The dissociation rate increases with temperature due to the increase in gluon density. The dissociation rate is maximum when the quarkonium is at rest and decreases with p_T.

3.3. Formation Rate

We can calculate the formation cross section from the dissociation cross section using detailed balance [62, 72],

$$\sigma_F = \frac{48}{36} \sigma_D(q^0) \frac{(s - M_Q^2)^2}{s(s - 4m_q^2)}. \tag{23}$$

The formation rate of quarkonium with momentum $\mathbf{p}$ can be written as

$$\frac{d\lambda_F}{d\mathbf{p}} = \int d^3p_1 \, d^3p_2 \, \sigma_F(s) \, v_{\rm rel}(s) \, f_q(p_1) \, f_{\bar{q}}(p_2) \, \delta(\mathbf{p} - (\mathbf{p_1} + \mathbf{p_2})). \tag{24}$$

Here $f_{q/\bar{q}}(p)$ are taken as thermal distribution function of $q/\bar{q}$ which are normalized to one, $\int f_q(p) d^3p = 1$ and $v_{\rm rel}$ is relative velocity of the $q\bar{q}$ quark pair,

$$v_{\rm rel} = \frac{\sqrt{(p_1.p_2)^2 - m_q^4}}{E_1 \, E_2}. \tag{25}$$

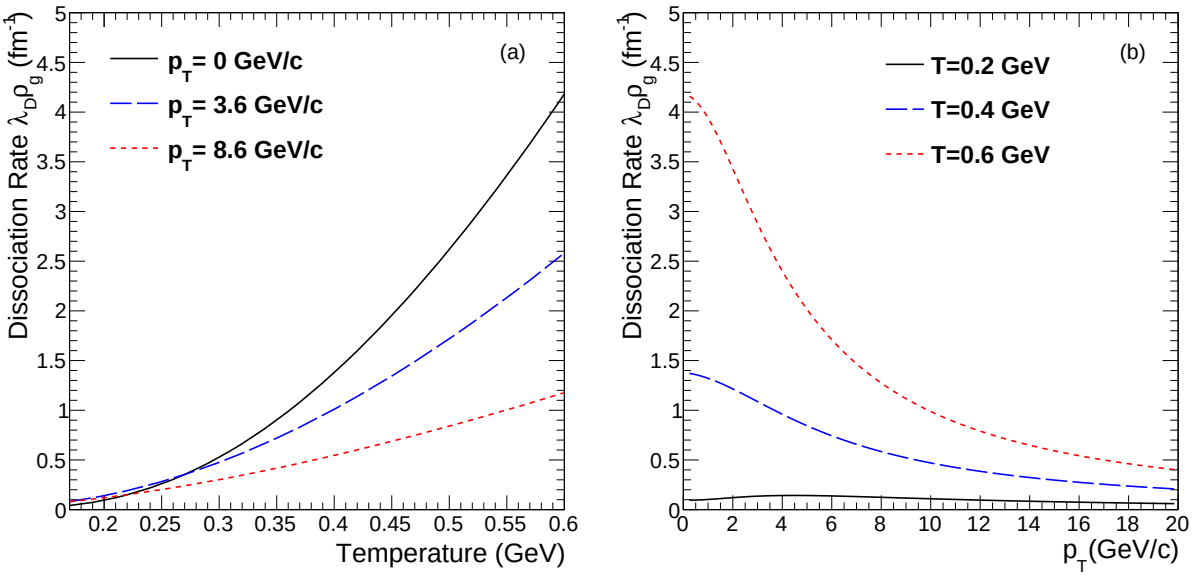

Figure 11: (Color online) Gluon dissociation rate of J/ψ as a function of (a) temperature and (b) transverse momentum.

Here $p_1 = (E_1, \mathbf{p_1})$ and $p_2 = (E_2, \mathbf{p_2})$ are the four momenta of the heavy quark and antiquark respectively. Figure 12 (a) shows the variation of the formation rate as a function of T and Fig. 12 (b) shows as a function of J/ψ p_T. The J/ψ generated from recombination of uncorrelated heavy quark pairs will have softer p_T distributions than those of J/ψ's coming from the initial hard scatterings. Thus the effect of recombination will be important only at low p_T.

Figure 13 (a) demonstrates the contributions from different processes to the centrality dependence of the Υ(1S) nuclear modification factor, along with the midrapidity data from CMS [73]. The calculations underestimate the suppression but reproduce the shape of centrality dependence. This may be due to the feed down effects from the excited states. Figure 13 (b) shows the same for the Υ(2S) nuclear modification factor along with the CMS measurements at midrapidity. The excited Υ(2S) states are highly suppressed. The effect of regeneration, not shown, is negligible for the Υ states. Figure 14 shows the forward rapidity ALICE measurement of the Υ(1S) nuclear modification factor [74] along with our calculations. The suppression due to thermal gluon dissociation is smaller than the measured suppression which may be due to the effect of feed down from the Υ(2S) and higher states. However the measurement is consistent with the suppression of Υ(2S) and Υ(3S) contribution, along with suppression of the Υ(1S) by gluon dissociation.

Figure 15(a) and (b) show the calculations of contributions to the nuclear modification factor, R_{AA}, for the Υ(1S) and Υ(2S) respectively as a function of p_T compared with the mid rapidity measurements from CMS [30]. The gluon dissociation mechanism combined with the pion dissociation and shadowing corrections gives good description of data in mid p_T range ($p_T \approx$ 5-10 GeV/c) for both Υ(1S) and Υ(2S). The contribution from the regenerated Υs is negligible even at LHC energies. Our calculations under-predict the suppression observed at the highest measured p_T for Υ(1S) and Υ(2S) which is similar for the case of J/ψ. The states Υ(1S) and Υ(2S) also have feed-down contributions from decays of higher b$\bar{\text{b}}$ bound states. The nuclear modification factor, R_{AA} is obtained taking into account the feed-down corrections as follows

$$R_{AA}^{\Upsilon(3S)} = R_{AA}^{\Upsilon(3S)} \tag{26}$$

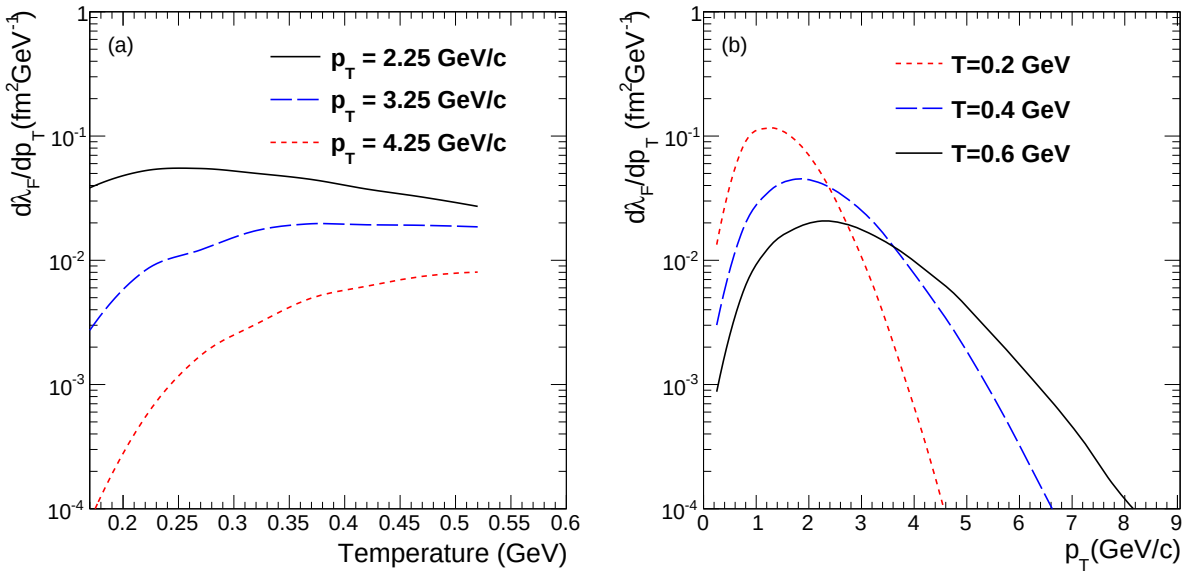

Figure 12: (Color online) Formation rate of J/ψ as a function of (a) temperature and (b) transverse momentum.

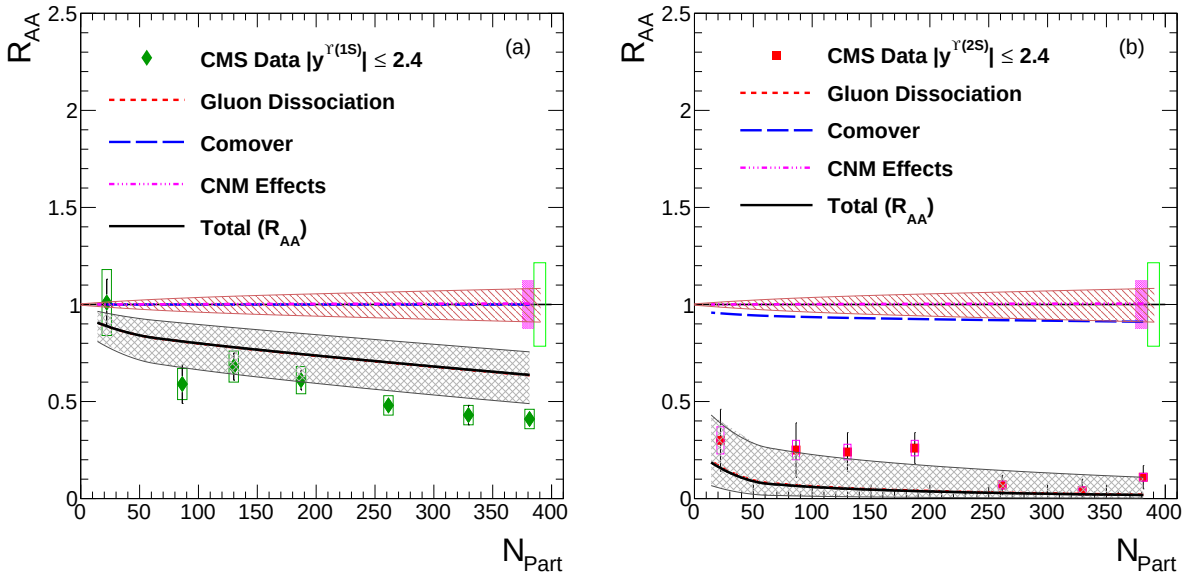

Figure 13: (Color online) Calculated nuclear modification factor (R_{AA}) compared with CMS (a) Υ(1S) and (b) Υ(2S) measurements. Regeneration is assumed to be negligible.

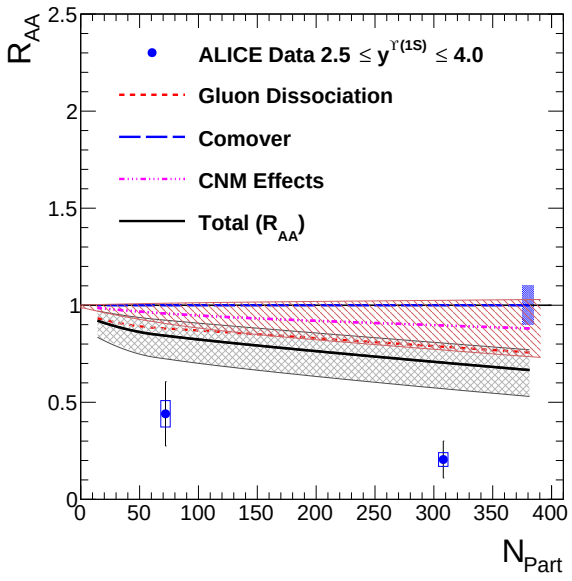

Figure 14: (Color online) Calculated nuclear modification factor (R_{AA}) compared with ALICE Υ(1S) measurement in forward rapidity.

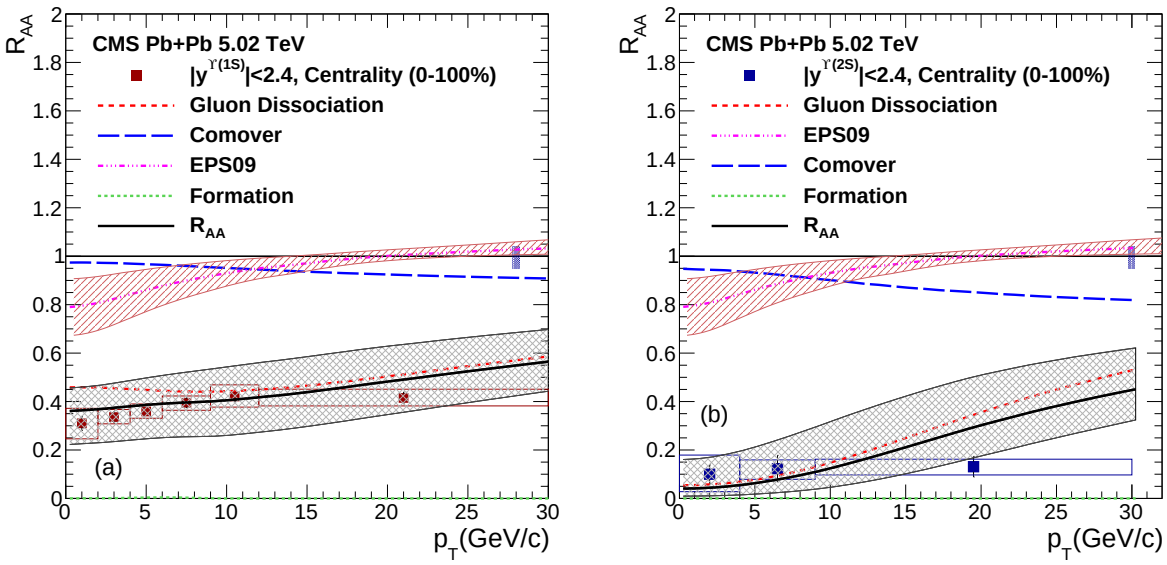

Figure 15: (Color online) Calculated nuclear modification factor (R_{AA}) of (a) Υ(1S) and (b) Υ(2S) as a function of p_T compared with CMS measurements [30]. The global uncertainty in R_{AA} is shown as a band around the line at 1.

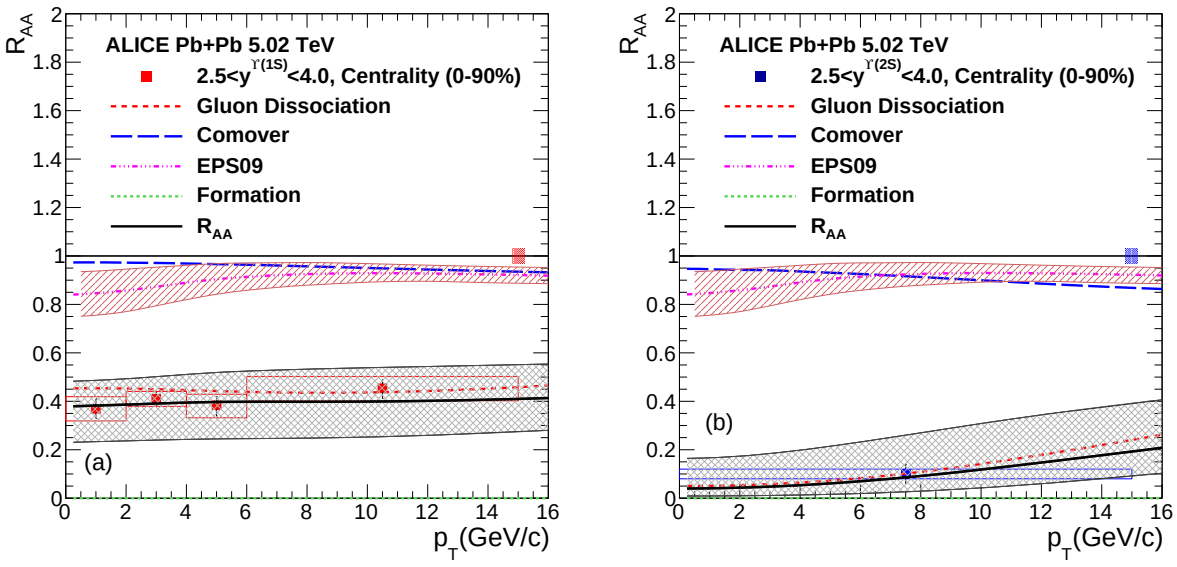

Figure 16: (Color online) Calculated nuclear modification factor (R_{AA}) of (a) Υ(1S) and (b) Υ(2S) as a function of p_T in the kinematic range of ALICE detector at LHC [**?**]. The global uncertainty in R_{AA} is shown as a band around the line at 1.

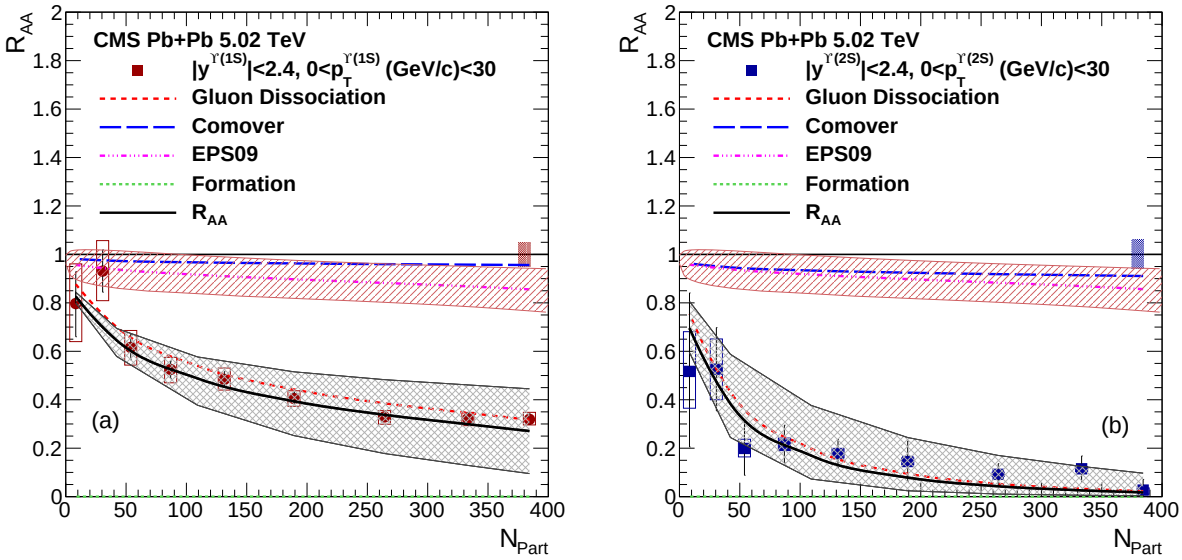

Figure 17: (Color online) Calculated nuclear modification factor (R_{AA}) of (a) Υ(1S) and (b) Υ(2S) as a function of centrality of the collisions compared with the CMS measurements [30].The global uncertainty in R_{AA} is shown as a band around the line at 1.

$$R_{AA}^{\Upsilon(2S)} = f_1 R_{AA}^{\Upsilon(2S)} + f_2 R_{AA}^{\Upsilon(3S)} \tag{27}$$

$$R_{AA}^{\Upsilon(1S)} = g_1 R_{AA}^{\Upsilon(1S)} + g_2 R_{AA}^{\chi_b(1P)} + g_3 R_{AA}^{\Upsilon(2S)} + g_4 R_{AA}^{\Upsilon(3S)} \tag{28}$$

The factors f's and g's are obtained from CDF measurement [75]. The values of g_1, g_2, g_3 and g_4 are 0.509, 0.27, 0.107 and 0.113 respectively. Here g_4 is assumed to be the combined fraction of Υ(3S) and χ_b(2P). The values of f_1 and f_2 are taken as 0.50 [76].

Figure 16(a) and (b) show the model prediction of the nuclear modification factor, R_{AA}, for the Υ(1S) and Υ(2S) respectively as a function of p_T in the kinematic range covered by ALICE detector. The ALICE data [**?**] is well described by our model.

Figure 17(a) depicts the calculated centrality dependence of the Υ(1S) nuclear modification factor, along with the midrapidity data from CMS [30]. Our calculations combined with the pion dissociation and shadowing corrections gives very good description of the measured data. Figure 17(b) shows the same for the Υ(2S) along with the midrapidity CMS measurements. The suppression of the excited Υ(2S) states is also well described by our model. As stated earlier, the effect of regeneration is negligible for Υ states.

Figure **??**(a) shows the forward rapidity ALICE measurement of the Υ(1S) nuclear modification factor [**?**] along with our calculations. The suppression due to thermal gluon dissociation describes the measured data after including the comover and shadowing corrections. Figure **??**(b) shows the calculations for the Υ(2S) nuclear modification factor in ALICE detector kinematic range. The suppression due to thermal gluon dissociation describes the ALICE measurements after including the comover and shadowing corrections.

3.3.1. Statistical (re) generation models

We can include the regenration part from our calculations. These effects are also small.

3.3.2. Comover models

The suppression of quarkonia by comoving pions can be calculated by folding the quarkonium-pion dissociation cross section $\sigma_{\pi Q}$ over thermal pion distributions [77]. It is expected that at LHC energies, the comover cross section will be small [78]. The pion-quarkonia cross section is calculated by convoluting the gluon-quarkonia cross section σ_D over the gluon distribution inside the pion [71],

$$\sigma_{\pi Q}(p_\pi) = \frac{p_+^2}{2(p_\pi^2 - m_\pi^2)} \int_0^1 dx\, G(x)\, \sigma_D(x p_+/\sqrt{2}), \tag{29}$$

where $p_+ = (p_\pi + \sqrt{p_\pi^2 - m_\pi^2})/\sqrt{2}$. The gluon distribution, $G(x)$, inside a pion is given by the GRV parameterization [79]. The pion momentum p_π is related to center of mass energy $\sqrt{s}$ of pion-J/ψ system by $p_\pi = (s - M_Q^2 - m_\pi^2)/(2M_Q)$. The dissociation rate λ_{D_π} can be written as

$$\begin{aligned} \lambda_{D_\pi}\, \rho_\pi &= \frac{g_\pi}{(2\pi)^3} \int d^3p_\pi f_\pi(p) \sigma_{\pi Q}(s) v_{\rm rel}(s) \\ &= \frac{g_\pi}{(2\pi)^3} \int dp_\pi\, 2\pi p_\pi^2 f_\pi(p_\pi) \int d\cos\theta\, \sigma_{\pi Q}(s)\, v_{\rm rel}(s) \Theta(s - 4m_D^2), \end{aligned} \tag{30}$$

where $f_\pi(p_\pi, T)$ is the thermal pion distribution. The pion density ρ_π is

$$\rho_\pi = \frac{g_\pi}{(2\pi)^3} \int d^3p_\pi \, f_\pi(p_\pi). \tag{31}$$

The survival probability from pion collisions at freeze-out time τ_f is written as

$$S_\pi(p_T) = \exp\left(- \int_{\tau_0}^{\tau_f} d\tau \, (1 - f(\tau)) \lambda_{D_\pi}(T, p_T) \, \rho_\pi(T) \right). \tag{32}$$

The hadronic fraction (1-$f(\tau)$) is zero in QGP phase. The probability $S_\pi(p_T)$ multiplies $S(p_T)$ in Eq. (13).

3.3.3. Summary of theoretical models for experimental comparison

We will write the summary for all different type of quarkonia model here.

3.4. Experimental overview of Bottomonia results at RHIC and LHC

3.4.1. Υ(nS) R_{AA} at the LHC

Measurement by CMS, ATLAS and ALICE. The bottomonia states (Υ(nS)) are measured at the LHC with very good statistical precision [**?** 73, 74**?**]. The CMS measurements at =2.76 TeV [**?** 73] reveal a clear proof of sequential suppression : Υ(2S) and Υ(3S) are more suppressed relative to the ground state Υ(1S). The individual Υ states are also found to be suppressed in the PbPb collisions relative to the production in the pp collisions. The Υ nuclear modification factor, R_{AA}, shows a strong dependence on collision centrality but has weak dependence on Υ meson and rapidity [**?**]. The forward rapidity ($2.5 \leq y^\Upsilon \leq 4.0$) measurement of the Υ suppression at ALICE [74] is found to be consistent with the midrapidity ($|y^\Upsilon| \leq 2.4$) measurement of the Υ suppression at the CMS. The CMS and ALICE collaborations have carried out the R_{AA} measurement of Υ at = 5.02 TeV with the Run II LHC PbPb collisions [**?** 30**?**]. The CMS experiment measured slightly more amount of Υ suppression at = 5.02 TeV [**?** 30] than the suppression at = 2.76 TeV [**?**] while the ALICE experiment observed less suppression at = 5.02 TeV than that at = 2.76 TeV in the most central PbPb collisions [74**?**].

3.4.2. Υ(nS) azimuthal anisotropy at the LHC

Measurement by CMS and ATLAS.

3.4.3. Υ(nS) R_{AA} at the RHIC

Measurement by STAR and PHENIX.

3.4.4. Summary and outlook

This will include comparison of RHIC and LHC results and then overview.

4. Conclusions and oulook

References

[1] E. V. Shuryak, Quantum Chromodynamics and the Theory of Superdense Matter, Phys. Rept. 61 (1980) 71–158. doi:10.1016/0370-1573(80)90105-2.

[2] H. Satz, The Quark-Gluon Plasma: A Short Introduction, Nucl. Phys. A 862-863 (2011) 4–12. arXiv:1101.3937, doi:10.1016/j.nuclphysa.2011.05.014.

[3] H. Satz, Color deconfinement in nuclear collisions, Rept. Prog. Phys. 63 (2000) 1511. arXiv:hep-ph/0007069, doi:10.1088/0034-4885/63/9/203.

[4] T. Matsui, H. Satz, J/ψ Suppression by Quark-Gluon Plasma Formation, Phys. Lett. B 178 (1986) 416–422. doi:10.1016/0370-2693(86)91404-8.

[5] L. Kluberg, 20 years of J/psi suppression at the CERN SPS: Results from experiments NA38, NA51 and NA50, Eur. Phys. J. C 43 (2005) 145–156. doi:10.1140/epjc/s2005-02245-6.

[6] P. Nason, S. Dawson, R. K. Ellis, The Total Cross-Section for the Production of Heavy Quarks in Hadronic Collisions, Nucl. Phys. B 303 (1988) 607–633. doi:10.1016/0550-3213(88)90422-1.

[7] P. Nason, S. Dawson, R. K. Ellis, The One Particle Inclusive Differential Cross-Section for Heavy Quark Production in Hadronic Collisions, Nucl. Phys. B 327 (1989) 49–92, [Erratum: Nucl.Phys.B 335, 260–260 (1990)]. doi:10.1016/0550-3213(89)90286-1.

[8] G. T. Bodwin, E. Braaten, G. P. Lepage, Rigorous QCD analysis of inclusive annihilation and production of heavy quarkonium, Phys. Rev. D 51 (1995) 1125–1171, [Erratum: Phys.Rev.D 55, 5853 (1997)]. arXiv:hep-ph/9407339, doi:10.1103/PhysRevD.55.5853.

[9] N. Brambilla, et al., Heavy quarkonium physicsarXiv:hep-ph/0412158, doi:10.5170/CERN-2005-005.

[10] M. B. Einhorn, S. D. Ellis, Hadronic Production of the New Resonances: Probing Gluon Distributions, Phys. Rev. D 12 (1975) 2007. doi:10.1103/PhysRevD.12.2007.

[11] S. D. Ellis, M. B. Einhorn, C. Quigg, Comment on Hadronic Production of Psions, Phys. Rev. Lett. 36 (1976) 1263. doi:10.1103/PhysRevLett.36.1263.

[12] C. E. Carlson, R. Suaya, Hadronic Production of psi/J Mesons, Phys. Rev. D 14 (1976) 3115. doi:10.1103/PhysRevD.14.3115.

[13] E. L. Berger, D. L. Jones, Inelastic Photoproduction of J/psi and Upsilon by Gluons, Phys. Rev. D 23 (1981) 1521–1530. doi:10.1103/PhysRevD.23.1521.

[14] G. A. Schuler, Quarkonium production and decays, Ph.D. thesis, Hamburg U. (1994). arXiv:hep-ph/9403387.

[15] P. Artoisenet, J. P. Lansberg, F. Maltoni, Hadroproduction of J/ψ and Υ in association with a heavy-quark pair, Phys. Lett. B 653 (2007) 60–66. arXiv:hep-ph/0703129, doi:10.1016/j.physletb.2007.04.031.

[16] J. M. Campbell, F. Maltoni, F. Tramontano, QCD corrections to J/psi and Upsilon production at hadron colliders, Phys. Rev. Lett. 98 (2007) 252002. arXiv:hep-ph/0703113, doi:10.1103/PhysRevLett.98.252002.

[17] P. Artoisenet, J. M. Campbell, J. P. Lansberg, F. Maltoni, F. Tramontano, Υ Production at Fermilab Tevatron and LHC Energies, Phys. Rev. Lett. 101 (2008) 152001. arXiv:0806.3282, doi:10.1103/PhysRevLett.101.152001.

[18] H. Fritzsch, Producing Heavy Quark Flavors in Hadronic Collisions: A Test of Quantum Chromodynamics, Phys. Lett. B 67 (1977) 217–221. doi:10.1016/0370-2693(77)90108-3.

[19] J. F. Amundson, O. J. P. Eboli, E. M. Gregores, F. Halzen, Colorless states in perturbative QCD: Charmonium and rapidity gaps, Phys. Lett. B 372 (1996) 127–132. arXiv:hep-ph/9512248, doi:10.1016/0370-2693(96)00035-4.

[20] J. F. Amundson, O. J. P. Eboli, E. M. Gregores, F. Halzen, Quantitative tests of color evaporation: Charmonium production, Phys. Lett. B 390 (1997) 323–328. arXiv:hep-ph/9605295, doi:10.1016/S0370-2693(96)01417-7.

[21] H.-L. Lai, M. Guzzi, J. Huston, Z. Li, P. M. Nadolsky, J. Pumplin, C. P. Yuan, New parton distributions for collider physics, Phys. Rev. D 82 (2010) 074024. arXiv:1007.2241, doi:10.1103/PhysRevD.82.074024.

[22] R. E. Nelson, R. Vogt, A. D. Frawley, Narrowing the uncertainty on the total charm cross section and its effect on the J/ψ cross section, Phys. Rev. C 87 (1) (2013) 014908. arXiv:1210.4610, doi:10.1103/PhysRevC.87.014908.

[23] M. Cacciari, P. Nason, R. Vogt, QCD predictions for charm and bottom production at RHIC, Phys. Rev. Lett. 95 (2005) 122001. arXiv:hep-ph/0502203, doi:10.1103/PhysRevLett.95.122001.

[24] K. J. Eskola, H. Paukkunen, C. A. Salgado, EPS09: A New Generation of NLO and LO Nuclear Parton Distribution Functions, JHEP 04 (2009) 065. arXiv:0902.4154, doi:10.1088/1126-6708/2009/04/065.

[25] V. Kumar, P. Shukla, R. Vogt, Components of the dilepton continuum in Pb+Pb collisions at $\sqrt{s_{NN}} = 2.76$ TeV, Phys. Rev. C 86 (2012) 054907. arXiv:1205.3860, doi:10.1103/PhysRevC.86.054907.

[26] S. Chatrchyan, et al., Observation and studies of jet quenching in PbPb collisions at nucleon-nucleon center-of-mass energy = 2.76 TeV, Phys. Rev. C 84 (2011) 024906. arXiv:1102.1957, doi:10.1103/PhysRevC.84.024906.

[27] B. Povh, K. Rith, C. Scholz, F. Zersche, W. Rodejohann, Particles and nuclei: An Introduction to the physical concepts, Graduate Texts in Physics, Springer, 1995. doi:10.1007/3-540-36684-9.

[28] S. M. Ikhdair, R. Sever, A Systematic study on nonrelativistic quarkonium interaction, Int. J. Mod. Phys. A 21 (2006) 3989–4002. arXiv:hep-ph/0508144, doi:10.1142/S0217751X06030953.

[29] A. M. Sirunyan, et al., Measurement of prompt and nonprompt charmonium suppression in PbPb collisions at 5.02 TeV, Eur. Phys. J. C 78 (6) (2018) 509. arXiv:1712.08959, doi:10.1140/epjc/s10052-018-5950-6.

[30] A. M. Sirunyan, et al., Measurement of nuclear modification factors of Υ(1S), Υ(2S), and Υ(3S) mesons in PbPb collisions at $\sqrt{s_{\mathrm{NN}}}$ = 5.02 TeV, Phys. Lett. B 790 (2019) 270–293. arXiv:1805.09215, doi:10.1016/j.physletb.2019.01.006.

[31] S. Acharya, et al., Studies of J/ψ production at forward rapidity in Pb-Pb collisions at $\sqrt{s_{\mathrm{NN}}}$ = 5.02 TeV, JHEP 02 (2020) 041. arXiv:1909.03158, doi:10.1007/JHEP02(2020)041.

[32] S. Acharya, et al., Υ suppression at forward rapidity in Pb-Pb collisions at $\sqrt{s_{\mathrm{NN}}}$ = 5.02 TeV, Phys. Lett. B 790 (2019) 89–101. arXiv:1805.04387, doi:10.1016/j.physletb.2018.11.067.

[33] M. Strickland, Thermal υ_{1s} and chi_b1 suppression in $\sqrt{s_{NN}}$ = 2.76 TeV Pb-Pb collisions at the LHC, Phys. Rev. Lett. 107 (2011) 132301. arXiv:1106.2571, doi:10.1103/PhysRevLett.107.132301.

[34] T. Song, K. C. Han, C. M. Ko, Bottomonia suppression in heavy-ion collisions, Phys. Rev. C 85 (2012) 014902. arXiv:1109.6691, doi:10.1103/PhysRevC.85.014902.

[35] V. Kumar, P. Shukla, R. Vogt, Quarkonia suppression in PbPb collisions at $\sqrt{s_{NN}}$ = 2.76 TeV, Phys. Rev. C 92 (2) (2015) 024908. arXiv:1410.3299, doi:10.1103/PhysRevC.92.024908.

[36] V. Kumar, P. Shukla, A. Bhattacharyya, Suppression of quarkonia in PbPb collisions at $\sqrt{s_{NN}}$ = 5.02 TeV, J. Phys. G 47 (1) (2020) 015104. arXiv:1909.10785, doi:10.1088/1361-6471/ab51cf.

[37] N. Brambilla, et al., QCD and Strongly Coupled Gauge Theories: Challenges and Perspectives, Eur. Phys. J. C 74 (10) (2014) 2981. arXiv:1404.3723, doi:10.1140/epjc/s10052-014-2981-5.

[38] J. L. Domenech, M. A. Sanchis-Lozano, Bottomonium production at the Tevatron and the LHC, Phys. Lett. B 476 (2000) 65–72. arXiv:hep-ph/9911332, doi:10.1016/S0370-2693(00)00119-2.

[39] J. L. Domenech, M. A. Sanchis-Lozano, Results from bottomonia production at the Tevatron and prospects for the LHC, Nucl. Phys. B 601 (2001) 395–421. arXiv:hep-ph/0012296, doi:10.1016/S0550-3213(01)00053-0.

[40] B. Gong, J.-X. Wang, H.-F. Zhang, QCD corrections to Υ production via color-octet states at the Tevatron and LHC, Phys. Rev. D 83 (2011) 114021. arXiv:1009.3839, doi:10.1103/PhysRevD.83.114021.

[41] R. Sharma, I. Vitev, High transverse momentum quarkonium production and dissociation in heavy ion collisions, Phys. Rev. C 87 (4) (2013) 044905. arXiv:1203.0329, doi:10.1103/PhysRevC.87.044905.

[42] P. Sun, C. P. Yuan, F. Yuan, Heavy Quarkonium Production at Low Pt in NRQCD with Soft Gluon Resummation, Phys. Rev. D 88 (2013) 054008. arXiv:1210.3432, doi:10.1103/PhysRevD.88.054008.

[43] B. Gong, L.-P. Wan, J.-X. Wang, H.-F. Zhang, Complete next-to-leading-order study on the yield and polarization of $\Upsilon(1S, 2S, 3S)$ at the Tevatron and LHC, Phys. Rev. Lett. 112 (3) (2014) 032001. arXiv:1305.0748, doi:10.1103/PhysRevLett.112.032001.

[44] Y. Feng, B. Gong, L.-P. Wan, J.-X. Wang, An updated study of Υ production and polarization at the Tevatron and LHC, Chin. Phys. C 39 (12) (2015) 123102. arXiv:1503.08439, doi:10.1088/1674-1137/39/12/123102.

[45] H. Han, Y.-Q. Ma, C. Meng, H.-S. Shao, Y.-J. Zhang, K.-T. Chao, $\Upsilon(nS)$ and $\chi_b(nP)$ production at hadron colliders in nonrelativistic QCD, Phys. Rev. D 94 (1) (2016) 014028. arXiv:1410.8537, doi:10.1103/PhysRevD.94.014028.

[46] G.-M. Yu, Y.-B. Cai, Y.-D. Li, J.-S. Wang, Heavy quarkonium photoproduction in ultrarelativistic heavy ion collisions, Phys. Rev. C 95 (1) (2017) 014905, [Addendum: Phys.Rev.C 95, 069901 (2017)]. arXiv:1703.03194, doi:10.1103/PhysRevC.95.014905.

[47] D. Acosta, et al., Υ Production and Polarization in $p\bar{p}$ Collisions at $\sqrt{s} = 1.8$-TeV, Phys. Rev. Lett. 88 (2002) 161802. doi:10.1103/PhysRevLett.88.161802.

[48] R. Aaij, et al., Measurement of Upsilon production in pp collisions at $\sqrt{s}$ = 7 TeV, Eur. Phys. J. C 72 (2012) 2025. arXiv:1202.6579, doi:10.1140/epjc/s10052-012-2025-y.

[49] V. Khachatryan, et al., Measurements of the Υ(1S), Υ(2S), and Υ(3S) differential cross sections in pp collisions at $\sqrt{s} = 7$ TeV, Phys. Lett. B 749 (2015) 14–34. arXiv:1501.07750, doi:10.1016/j.physletb.2015.07.037.

[50] G. Aad, et al., Measurement of Upsilon production in 7 TeV pp collisions at ATLAS, Phys. Rev. D 87 (5) (2013) 052004. arXiv:1211.7255, doi:10.1103/PhysRevD.87.052004.

[51] S. Chatrchyan, et al., Measurement of the $\Upsilon(1S)$, $\Upsilon(2S)$, and $\Upsilon(3S)$ Cross Sections in pp Collisions at $\sqrt{s}$ = 7 TeV, Phys. Lett. B 727 (2013) 101–125. arXiv:1303.5900, doi:10.1016/j.physletb.2013.10.033.

[52] A. M. Sirunyan, et al., Measurement of quarkonium production cross sections in pp collisions at $\sqrt{s} = 13$ TeV, Phys. Lett. B 780 (2018) 251–272. arXiv:1710.11002, doi:10.1016/j.physletb.2018.02.033.

[53] P. A. Zyla, et al., Review of Particle Physics, PTEP 2020 (8) (2020) 083C01. doi:10.1093/ptep/ptaa104.

[54] V. Kumar, P. Shukla, Charmonia production in p + p collisions under NRQCD formalism, J. Phys. G 44 (8) (2017) 085003. arXiv:1606.08265, doi:10.1088/1361-6471/aa7818.

[55] R. Baier, R. Ruckl, Hadronic Collisions: A Quarkonium Factory, Z. Phys. C 19 (1983) 251. doi:10.1007/BF01572254.

[56] B. Humpert, NARROW HEAVY RESONANCE PRODUCTION BY GLUONS, Phys. Lett. B 184 (1987) 105–107. doi:10.1016/0370-2693(87)90496-5.

[57] R. Gastmans, W. Troost, T. T. Wu, Production of Heavy Quarkonia From Gluons, Nucl. Phys. B 291 (1987) 731. doi:10.1016/0550-3213(87)90493-7.

[58] P. L. Cho, A. K. Leibovich, Color octet quarkonia production, Phys. Rev. D 53 (1996) 150–162. arXiv:hep-ph/9505329, doi:10.1103/PhysRevD.53.150.

[59] P. L. Cho, A. K. Leibovich, Color octet quarkonia production. 2., Phys. Rev. D 53 (1996) 6203–6217. arXiv:hep-ph/9511315, doi:10.1103/PhysRevD.53.6203.

[60] T.-J. Hou, et al., New CTEQ global analysis of quantum chromodynamics with high-precision data from the LHC, Phys. Rev. D 103 (1) (2021) 014013. arXiv:1912.10053, doi:10.1103/PhysRevD.103.014013.

[61] A. Mocsy, P. Petreczky, M. Strickland, Quarkonia in the Quark Gluon Plasma, Int. J. Mod. Phys. A 28 (2013) 1340012. arXiv:1302.2180, doi:10.1142/S0217751X13400125.

[62] R. L. Thews, M. Schroedter, J. Rafelski, Enhanced J/ψ production in deconfined quark matter, Phys. Rev. C 63 (2001) 054905. arXiv:hep-ph/0007323, doi:10.1103/PhysRevC.63.054905.

[63] X. Zhao, R. Rapp, Medium Modifications and Production of Charmonia at LHC, Nucl. Phys. A 859 (2011) 114–125. arXiv:1102.2194, doi:10.1016/j.nuclphysa.2011.05.001.

[64] P. Huovinen, P. Petreczky, QCD Equation of State and Hadron Resonance Gas, Nucl. Phys. A 837 (2010) 26–53. arXiv:0912.2541, doi:10.1016/j.nuclphysa.2010.02.015.

[65] K. Aamodt, et al., Centrality dependence of the charged-particle multiplicity density at mid-rapidity in Pb-Pb collisions at $\sqrt{s_{NN}} = 2.76$ TeV, Phys. Rev. Lett. 106 (2011) 032301. arXiv:1012.1657, doi:10.1103/PhysRevLett.106.032301.

[66] S. Chatrchyan, et al., Dependence on pseudorapidity and centrality of charged hadron production in PbPb collisions at a nucleon-nucleon centre-of-mass energy of 2.76 TeV, JHEP 08 (2011) 141. arXiv:1107.4800, doi:10.1007/JHEP08(2011)141.

[67] E. V. Shuryak, Two stage equilibration in high-energy heavy ion collisions, Phys. Rev. Lett. 68 (1992) 3270–3272. doi:10.1103/PhysRevLett.68.3270.

[68] E. Abbas, et al., Centrality dependence of the pseudorapidity density distribution for charged particles in Pb-Pb collisions at $\sqrt{s_{\rm NN}}$ = 2.76 TeV, Phys. Lett. B 726 (2013) 610–622. arXiv:1304.0347, doi:10.1016/j.physletb.2013.09.022.

[69] G. Bhanot, M. E. Peskin, Short Distance Analysis for Heavy Quark Systems. 2. Applications, Nucl. Phys. B 156 (1979) 391–416. doi:10.1016/0550-3213(79)90200-1.

[70] F. Karsch, M. T. Mehr, H. Satz, Color Screening and Deconfinement for Bound States of Heavy Quarks, Z. Phys. C 37 (1988) 617. doi:10.1007/BF01549722.

[71] F. Arleo, P. B. Gossiaux, T. Gousset, J. Aichelin, Heavy quarkonium hadron cross-section in QCD at leading twist, Phys. Rev. D 65 (2002) 014005. arXiv:hep-ph/0102095, doi:10.1103/PhysRevD.65.014005.

[72] R. L. Thews, M. L. Mangano, Momentum spectra of charmonium produced in a quark-gluon plasma, Phys. Rev. C 73 (2006) 014904. arXiv:nucl-th/0505055, doi:10.1103/PhysRevC.73.014904.

[73] S. Chatrchyan, et al., Observation of Sequential Upsilon Suppression in PbPb Collisions, Phys. Rev. Lett. 109 (2012) 222301, [Erratum: Phys.Rev.Lett. 120, 199903 (2018)]. arXiv:1208.2826, doi:10.1103/PhysRevLett.109.222301.

[74] B. B. Abelev, et al., Suppression of $\Upsilon(1S)$ at forward rapidity in Pb-Pb collisions at $\sqrt{s_{\rm NN}} = 2.76$ TeV, Phys. Lett. B 738 (2014) 361–372. arXiv:1405.4493, doi:10.1016/j.physletb.2014.10.001.

[75] T. Affolder, et al., Production of $\Upsilon(1S)$ mesons from χ_b decays in $p\bar{p}$ collisions at $\sqrt{s} = 1.8$ TeV, Phys. Rev. Lett. 84 (2000) 2094–2099. arXiv:hep-ex/9910025, doi:10.1103/PhysRevLett.84.2094.

[76] M. Strickland, D. Bazow, Thermal Bottomonium Suppression at RHIC and LHC, Nucl. Phys. A 879 (2012) 25–58. arXiv:1112.2761, doi:10.1016/j.nuclphysa.2012.02.003.

[77] R. Vogt, M. Prakash, P. Koch, T. H. Hansson, J/ψ Interactions With Hot Hadronic Matter, Phys. Lett. B 207 (1988) 263–268. doi:10.1016/0370-2693(88)90572-2.

[78] C. Lourenco, R. Vogt, H. K. Woehri, Energy dependence of J/psi absorption in proton-nucleus collisions, JHEP 02 (2009) 014. arXiv:0901.3054, doi:10.1088/1126-6708/2009/02/014.

[79] M. Gluck, E. Reya, A. Vogt, Pionic parton distributions, Z. Phys. C 53 (1992) 651–656. doi:10.1007/BF01559743.